Seeding effects of submicron CaAl-NO_3 LDH particles on the hydration and properties of Portland cement and sulfoaluminate cement pastes.

Sukanta K. Mondal[a], Monday U. Okoronkwo[a,b,*]

[1]Linda and Bipin Doshi Department of Chemical and Biochemical Engineering, Missouri University of Science and Technology, Rolla, Missouri 65409, United States
[2]Sustainable Materials Laboratory (SusMatLab), Missouri University of Science and Technology, Rolla, Missouri 65409, United States
*Corresponding author: Monday U. Okoronkwo, okoronkwom@mst.edu, Phone: 573-341-4349

Abstract:
Layered double hydroxide (LDH) is reported to improve the durability of concretes, primarily due to its ability to exchange anionic species, including chloride, which is implicated in corrosion-driven durability issues. However, there is no comprehensive study investigating the effect of LDH on the properties of different cement systems at both early and mature ages. In this study, the early age and mature age properties of Portland cement (OPC) and calcium sulfoaluminate (CSA) cement pastes seeded with submicron-sized calcium aluminum-NO_3 LDH (CaAl-NO_3 LDH) were investigated. The effects of the 1- 5 $\%_{mass}$ dosage of LDH on the hydration of both cement systems were characterized by rheology, isothermal calorimetry, porosimetry, compressive strength tests, thermogravimetric analysis, and x-ray diffraction. Time-dependent rheology results indicate that CaAl-NO_3 LDH seeding enhanced the buildability of cement pastes, as evidenced by increased plasticity loss, hardening, and yield stress. While LDH seeding accelerated hydration kinetics for both CSA and OPC pastes, interestingly, the OPC exhibited reduced heat release, suggesting potential applications of LDH as heat sink in various areas, including building in hot climates, reducing heat and crack-propensity in mass concrete placements, and 3D-printed OPC-based concretes. Although LDH slightly decreased compressive strengths at both 1d and 28d, its primary role was to expedite the hydration process without enhancing the microstructure or strength of the final product.

Keywords: Calcium sulfoaluminate cement; Layered double hydroxide; Chemical admixtures; Rheology; AFm phase; Portland cement.

1. Introduction

Layered double hydroxides (LDHs) are 2D materials, also known as ionic solids with exchangeable anionic layers sandwiched by a brucite-like double-layer structure [1–3]. A portion of the divalent cations in the structure are coordinated with oxygens to form the octahedra structure, and when their edges are shared, they create thin 2D infinite layers. A positive charge is produced on the layers when trivalent cations are partially and isomorphously substituted for divalent ones. The positively charged 2D layers are separated by the charge-balancing anions, and any remaining space in the interlayer area may be taken up by hydrogen-bonded water molecules. A general formula of LDHs is $[M^{2+}_{1-x}M^{3+}_{x}(OH)_2]^{x+}(A^{n-})_{x/n}\cdot mH_2O$, where the exchangeable anions are represented by A^{n-} (e.g., NO_3^-, Cl^-, CO_3^{2-}), and x is the molar ratio of M^{3+} / (M^{3+} + M^{2+}) [M^{2+} = Ca^{2+}, Mg^{2+}, Zn^{2+} etc., and M^{3+}= Al^{3+}, Fe^{3+}, Cr^{3+} etc.] [4,5].

In recent years, multifunctional LDH materials have gained increasing interest in many applications. The weak electrostatic force between anions in the interlayer and the cationic layers makes it easy to exchange the interlayer anions wherein the ability of the anions to replace each other follow the sequence of ($CO_3^{2-} > SO_4^{2-} > OH^- > NO_3^-$) [6]. Due to its ion-exchange capability, high tunability, and easy methods for synthesis, LDH have been adapted for many significant applications, including catalysis [7,8], ion-exchange [9], adsorption [10–12], pharmaceutics [13,14], biochemistry [15], genetic engineering [16], electrochemistry [17–19], corrosion protection [20–22], polymer materials [23–25], cement and concrete systems [26–32], etc. Furthermore, the synthesis of LDHs is inexpensive and straightforward in both laboratory and industrial scales, positioning LDH-based materials as eco-friendly and cost-effective multifunctional material [33–35]. In the realm of cement and construction materials, the addition of LDH stands out for their cost-effectiveness and eco-friendliness, as their addition enhances the durability and performance of cementitious matrices. Also, it may potentially reduce the need for less benign synthetic additives, and promote the utilization of industrial by-products [36].

Among many other types of LDHs, CaAl-NO_3 LDH has some critical benefits. Firstly, as from the sequence above, the NO_3^- can easily be exchanged by anionic polymer (e.g., PCE), and some of the harmful anions (e.g., Cl^-, CO_3^{2-}), thereby facilitating the removal of deleterious ions such as Cl^-, CO_3^{2-} and release of nitrate into the pore solution which can make the cement hydration process smoother and protect steel reinforcement from corrosion in the concrete system [22]. Secondly, unlike some non-native nano and submicron particles (e.g., titania, clay, copper, carbon-based materials, etc.) [37] that are frequently used to enhance the hydration and properties of cement-based materials, LDHs (popularly known as AFm phases in cement community) [38–43] are native to cement system which helps with the additive stability and compatibility in the cement systems. Hence, the CaAl-NO_3 LDH variant was the main focus of the present study to understand its seeding effects on the early age and mature age properties of both CSA cements and Portland cement (OPC).

OPC dominates global cement usage, but enhancing its workability remains crucial for specific applications like 3D printing and oil-well cementing. As cement production contributes ~ 8% of global CO_2 emission, there is a rising interest in sustainable alternatives like CSA cement, which closely competes with OPC in performance and research attention. Inclusion of LDH in the OPC and CSA cement systems is not new, but the published studies are limited to certain aspects. There are scarce studies which thoroughly investigated the effect of LDH (e.g., CaAl-NO_3 LDH) in both OPC and CSA cement systems. Investigating the impact of LDH in both OPC and CSA cement systems holds critical importance, as OPC is the most widely utilized cement, and CSA is emerging as a highly promising alternative, offering a more sustainable solution. Understanding their individual interactions with LDH is crucial for optimizing their respective performances and advancing sustainable construction practices [6,44–48].
In cement systems, most of the available studies are limited to the effectiveness of LDHs in corrosion protection [20–22], improvement of mechanical strength [49–51,51], and controlled admixture release [26,28,32,52,53]. Further investigation into the impact of LDH addition on

cement paste hydration, time-dependent workability, and microstructural-to-bulk properties development is still crucial. This study provides some of the critical aspects and findings on the incorporation of LDH in the above two types of cement pastes (OPC and CSA cement), providing insights on the effectiveness of LDH in cement systems in 1) the presence of different chemical admixtures; and effects of LDH on the 2) time-dependent static and dynamic rheological behavior, 3) the heat evolution characteristics, 4) thermogravimetric changes, 5) time-dependent evolution of the hydrated phases, 6) porosity and pore structures, and 7) compressive strength development.

2. Experimental

2.1 Materials

2.1.1 Synthesis of CaAl-NO_3 LDH

The CaAl-NO_3 LDH was successfully synthesized by a pH-controlled coprecipitation technique following the published methods [28,54,55]. Analytical grade 66.122 g $Ca(NO_3)_2.4H_2O$ (calcium nitrate tetrahydrate, ACROS organics, purity of 98%) and 45.01 g $Al(NO_3)_3.9H_2O$ (aluminum nitrate nanohydrate, Alfa Aesar, purity of 98%) were mixed together at solid state. 320 ml deionized water (resistivity of 18.2 MΩ) was added to the mixed solids maintaining an overall liquid/solid ≈ 2. This solution was then poured dropwise into another mixed solids of 24 g NaOH (sodium hydroxide, Fisher chemical) and 34 g $NaNO_3$ (sodium nitrate, Alfa Aesar, purity of 99%) with stirring. The final pH of the solution was 9.1. The mixture was heated under insulation at 65 ^oC for 16 h maintaining a vigorous stirring at 800 rpm. The mixture was then filtered and thoroughly washed several times with decarbonated water and acetone. Finally, the LDH material was dried under vacuum (-27 inHg) for ~ 30 h.

The particle size distribution of the LDH sample was measured by a dynamic light scattering (DLS) instrument (Anton Paar Litesizer 500) as shown in **Fig. 1(a)**, and the average particle size from three runs was in the submicron range (< 1 μm) with a median size (D_{50}) of 0.39 μm. The X-ray diffraction (XRD) profile of the LDH acquired with a PANalytical X'Pert Pro diffractometer utilizing a 2θ configuration and CuKα (λ = 1.540 Å) radiation is presented in **Fig. 1(c)**. The morphology of the synthesized LDH surfaces was examined using a Hitachi S4700 scanning electron microscope (SEM) as shown in **Fig. 1 (b)**.

2.1.2 Cement samples and admixtures

A commercial grade OPC (Type I/II) and CSA cement was received from Continental Cement Co. USA, and Buzzi Unicem USA, respectively. The elemental oxide composition of the cement samples was analyzed with Rigaku Supermini 200 wavelength dispersive X-ray fluorescence and presented in **Table 1**. The XRD profiles of the OPC and CSA cement samples are shown in **Fig. 2**. The quantitative x-ray powder diffraction (QXRD)-based phase analysis indicates the CSA cement contains 41% ye'elimite, 29.2% belite, 27 % anhydrite, and 2.8% aluminate. The QXRD of OPC shows 70.2% alite, 22.5 % belite, 5.6% gypsum, 1.4% aluminate, 0.1% ferrite, and 0.2% periclase. Rietveld refinement method was utilized for QXRD analysis, with corundum as an internal standard at 10 wt% [56,57]. The QXRD results were obtained with Rwp of < 5%. The particle size of the CSA cement and OPC measured with the DLS technique were 2.21 μm and 3.4 μm, respectively.

A fixed dosage of reagent-grade citric acid (CA) monohydrate ($C_6H_8O_7 \cdot H_2O$, ACROS organics, purity of 99.5%) was used as a retarder for the CSA cement (CSAC) pastes, while a fixed dosage of Adva Cast 600 (GCP Applied Technologies, USA), a polycarboxylate ether (PCE)-based polymer dispersant compliant with ASTM C1017 Type I standards was utilized to enhance dispersion of particles in both the OPC and CSAC systems. It is often thought that competitive adsorption of PCE and citric acid, and the nature of the CSA cement systems, will make PCE ineffective when employed together with smaller citric molecule in CSA pastes[58]. To clarify these assumptions, some the CSA systems were studied with only citric acid admixture with no PCE in the formulation for comparison.

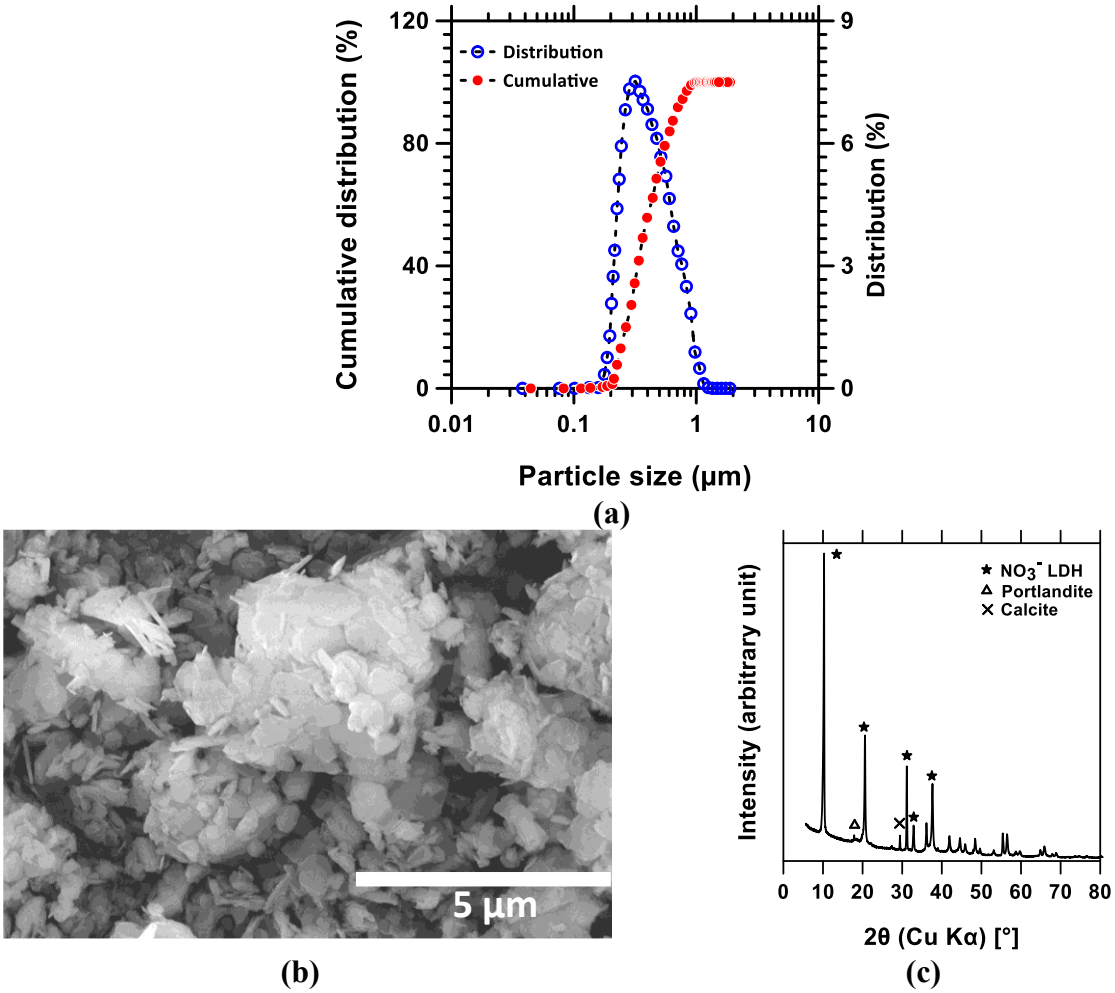

Fig. 1. (a) Average intensity weighted size distribution, **(b)** SEM image, and **(c)** XRD pattern of the of submicron CaAl-NO_3 LDH Particles.

Table 1. Elemental composition of cement samples ($\%_{mass}$).

Species	Na_2O	MgO	CaO	Al_2O_3	SiO_2	P_2O_5	SO_3	K_2O	TiO_2	MnO	Fe_2O_3	LOI
CSAC	0.29	0.74	48.60	20.44	13.31	0.38	10.01	0.61	0.56	0.10	3.22	1.65

OPC	0.10	2.07	64.40	3.55	19.28	0.01	1.18	0.9	0.34	0.75	3.9	3.35

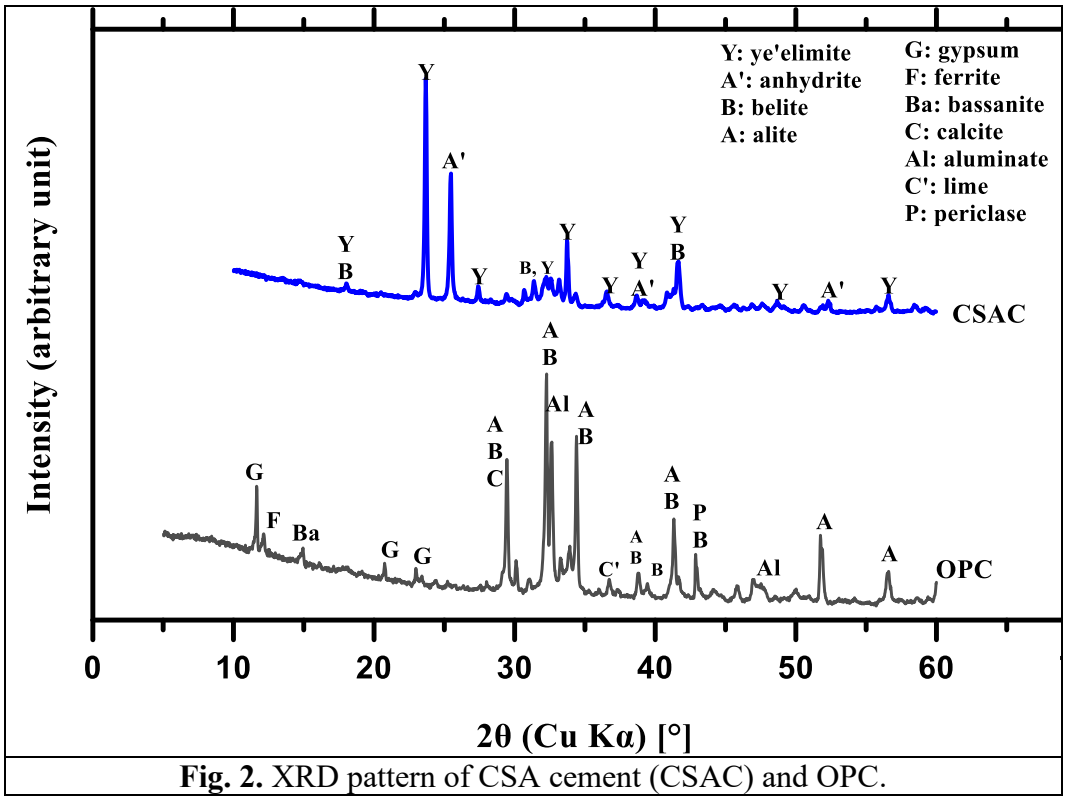

Fig. 2. XRD pattern of CSA cement (CSAC) and OPC.

2.2 Mixing protocol

For the rheology study, the mix designs for CSAC and OPC pastes were prepared with 1 – 5 $\%_{mass\ of\ dry\ cement}$ dosages of LDH at a constant water/cement (w/c, mass fraction) of 0.5. The 1-5 $\%_{mass}$ LDH was selected in this study to examine its broader impact on OPC and CSA cement systems, aiming to find an optimal balance that enhances properties without detrimental effects [6,59]. Two different types of CSA cement pastes were prepared for the rheology study: i) with PCE, and ii) without PCE. This was done to investigate the influence of PCE in these CSA cement systems. A set retarder was always used in both CSA mix designs. A dosage of 0.1$\%_{mass\ of\ cement}$ PCE and 2 $\%_{mass\ of\ cement}$ citric acid (CA) was used in this study, which was the optimum dosage in one of the previous studies [60]. The OPC pastes contained 0.1$\%_{mass\ of\ cement}$ PCE. The ratio of the admixtures in the mixture was maintained constant (on the basis of the cement mass only) in the pastes, whereas the dosage of the LDH was varied. The cement pastes were prepared using grade II deionized water. In the pastes, the total amount of the water employed was accounted including the water present in chemical admixtures. The mix proportions of different pastes are listed in **Table 2**. In case of the pastes without PCE, no PCE was used in the mix design.

Table 2. Mix proportions of cement pastes ($\%_{mass}$).

Cement	DI water	$C_6H_8O_7 \cdot H_2O$ (CA.H_2O)*	PCE (solid polymer basis)	LDH (1-5%)

10	4.98	0.22	0.01	0.1
10	4.98	0.22	0.01	0.2
10	4.98	0.22	0.01	0.3
10	4.98	0.22	0.01	0.4
10	4.98	0.22	0.01	0.5

*The citrate contributes 0.02g of water, making the net water content of 5g per 10g of cement.

For better dispersion of LDH in the cement pastes, the design proportion of LDH, PCE (without PCE for some of the CSA pastes), and water were mixed and sonicated for five minutes in a 30W Branson 200 ultrasonic cleaner with an output frequency of 46 KHz. In CSA systems, the desired blend ratios of the other solid components (CSA cement and citric acid powder) were initially homogenized manually before blending with the sonicated mixtures. In preparation for OPC pastes, the sonicated sample was mixed to the OPC cement. For each static rheology study, 10 g of cement was employed. Always, a 250 mL plastic container was used for preparing the pastes utilizing a IKA RW 20 Digital four-blade overhead stirrer for one minute of homogeneous mixing at 1000 rpm. The paste was immediately placed into the rheometer for the rheology measurements. A consistent mixing procedure was followed for preparing samples for hydrate phase assemblage tracking, compressive strength test cubes, and isothermal calorimetry tests. For calorimetry tests, the liquids were then introduced to the mixed solids in a 2 ml glass vial (National C4013-1W 12 x 32mm clear screw thread, Thermo Scientific), and the pastes were manually stirred for an additional minute. After that, the vial was placed into the micro reaction calorimeter for isothermal analysis.

2.3 Parallel plate rheometry of cement pastes

For analyzing the rheological behavior of the cement pastes, parallel plate geometries were preferred [61–65]. This study used a stress-controlled shear rheometer (DHR-2, TA Instruments) in a parallel plate configuration, utilizing 40 mm-diameter plates on both top and bottom to assess the evolving yield stress of the cement pastes over time. The top and bottom plate surfaces were crosshatched to reduce slippage and to keep a uniform distribution of cement particles near the plates [66]. Prior to each test, the inertia of the instrument, and the inertia and friction of the geometry were calibrated. For better comparison of the rheology data, the calibration results were ensured to be consistent with the previous calibration data.

During the run time, a 1000 μm gap was maintained between the upper and lower plates. Throughout the experiments, a constant temperature of 25 °C was maintained using a Peltier plate attached to the bottom geometry. During the tests, the pastes were covered from drought with the aid of an environmental chamber and a small amount of deionized (DI) water was placed in a solvent trap on the top plate to maintain a consistent humidity level surrounding the pastes. The same experimental set up was applied to assess both the static and dynamic rheological behavior of the pastes.

The time taken to mix and set up the paste sample on the rheometer was about five minutes from the moment the cement made contact with the liquid used for mixing (which contained LDH, water, and PCE). The pastes were sheared for 180 s with a rate of 0.01 s^{-1} after being pre-sheared

for 30 s at 0.1 s^{-1} followed by a 30 s rest. As shown in **Fig. 3 (a)**, the static yield stress was obtained as the peak shear stress where the paste started to flow. This transition point is where the elastic deformation changed to plastic flow, measured at a constant shear strain rate of 0.01 s^{-1} [60]. A reasonable estimate of the static yield stress is the peak shear stress [67,68]. **Fig. 3 (c)** shows a representative shear stress vs. shear rate curve, wherein the commonly used Bingham model, $\boldsymbol{\sigma^* = \sigma_y + \mu_{pl}.\dot{\gamma}}$, [where $\boldsymbol{\sigma^*}$ indicates the shear stress, $\boldsymbol{\sigma_y}$ is the yield stress, $\boldsymbol{\mu_{pl}}$ is the plastic viscosity, and $\boldsymbol{\dot{\gamma}}$ is the shear rate (0-200 s^{-1})], was applied on the ramp-down to extract the dynamic yield stress and plastic viscosity.

Fig. 3 (b) shows the representative evolution yield stress as a function of hydration time, where slopes $\boldsymbol{m_1}$ and $\boldsymbol{m_2}$ of the two linear regimes represents the paste's flowability loss rate and hardening rate, accordingly. The placement limit, $\boldsymbol{t_p}$, represents the endpoint of the plastic behavior or flowability regime of the pastes and where the hardening regime starts. In practical cement work, it is to be noted that before the $\boldsymbol{t_p}$, the cement mixture should have been be placed, and then the finishing completed promptly as the cement pastes loses its workability rapidly after $\boldsymbol{t_p}$ [69]. Additionally, the exponential growth model $\boldsymbol{\sigma_{y_t} = \sigma_{y_0} e^{kt}}$ can be applied to the yield stress data to understand the overall yield stress build-up kinetics, where $\boldsymbol{\sigma_{y_t}}$ is the yield stress at time t, $\boldsymbol{\sigma_{y_0}}$ is the initial yield stress first measured after mixing, and $\boldsymbol{k}$ is the yield stress growth rate constant[60].

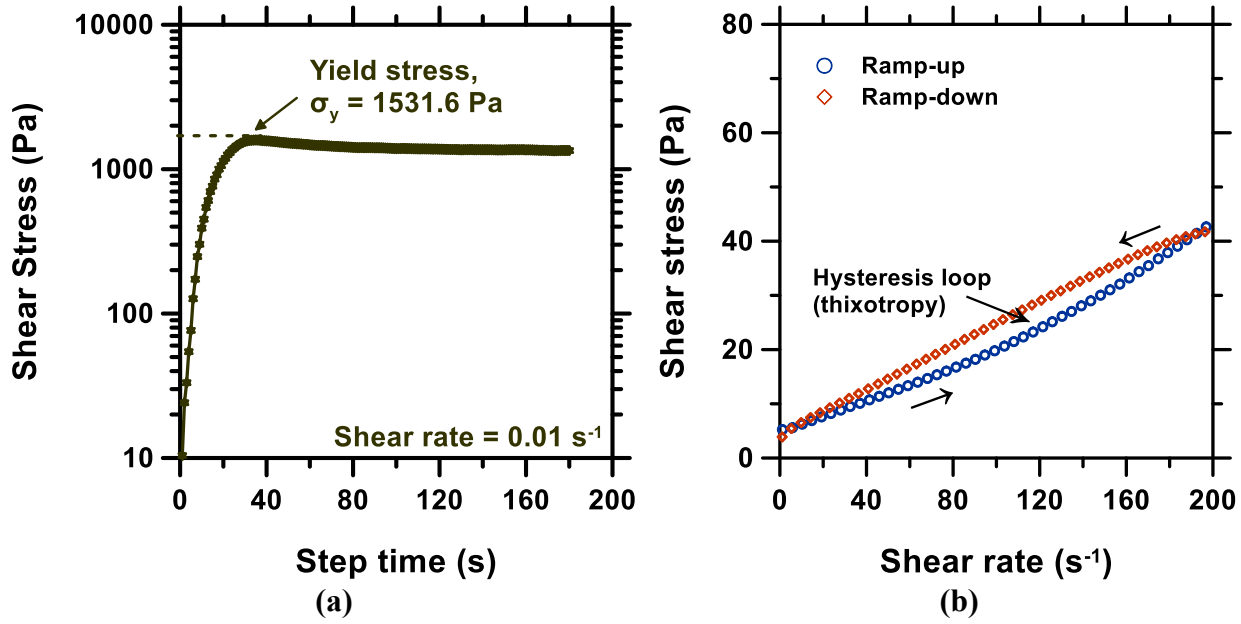

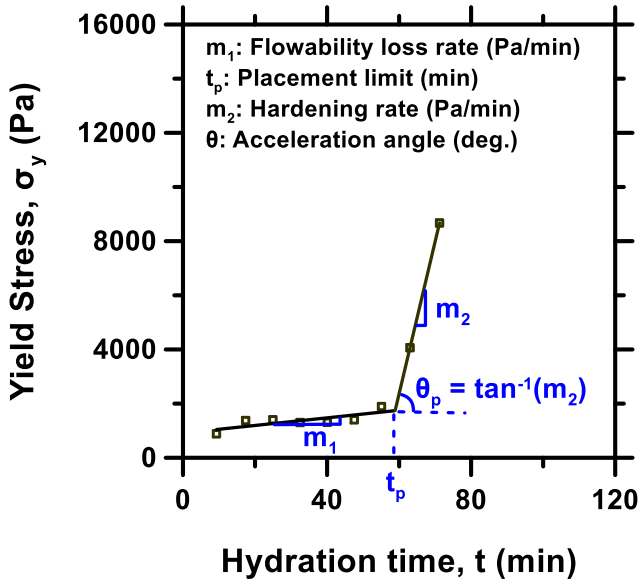

(c)

Fig. 3. Representative: **(a)** stress growth flow curve for determining the static yield stress (σ_y) was determined, **(b)** shear stress-shear rate flow curves showing the ramp-up and ramp-down between 0-200 s^{-1} for the determination of dynamic yield stress and plastic viscosity using the Bingham model on the down ramp, **(b)** time-dependent yield stress evolution of cement paste, illustrating the flowability loss rate $\boldsymbol{m_1}$, placement limit $\boldsymbol{t_p}$, acceleration angle $\boldsymbol{\theta_p}$, and hardening rate $\boldsymbol{m_2}$ workability parameters.

2.4. Isothermal calorimetry

A widely used approach for monitoring cement's hydration is isothermal calorimetry. For all the OPC and CSA cement pastes utilized for the rheology investigations, isothermal calorimetry was studied to investigate the seeding effects of the LDH on the hydration kinetics of the cement pastes. Utilizing a THT µRC single-channel isothermal micro reaction calorimeter with Peltier-based temperature control, the heat development, and the cumulative heat from the hydration of the cement systems were observed for 24 hours at a fixed temperature of 25 ± 0.001°C and at ambient pressure. In every test, 0.7 g sample of cement was used and the same mix design proportions, including w/c of 0.5 and 0.1%$_{\text{mass of cement}}$ PCE (plus 2%CA for CSAC pastes) were maintained for calorimetric measurement. The materials were placed within a 2.0 ml glass vial with a typical polypyridene cover before being loaded into the microcalorimeter. This research leverages the capability of the THT micro reaction calorimeter to identify heat evolution with a fairly high precision, having a resolution of 5 µW and a range between 5 µW and 600 mW. To reduce interference and undesirable transient effects, a neutral reference sample (equivalent water) vial with a heat capacity similar to the paste sample was incorporated into the reference cell [70]. All the isothermal experiments were initiated on stabilization at the set temperature, after 4.5 minutes of mixing the solid and liquid components.

2.5. Compressive strength tests

The 1d and 28d compressive strength of 0, 1, and 5% LDH-dosed OPC and CSA cement cubes were investigated to understand the effect of LDH and evolution of mechanical strength over time. The 1-inch cubes were prepared maintaining the same mix proportions stated in **section 2**.
The cubes were prepared and stored in accordance with ASTM C 109, C 305, and C 511-19 standards. A Perfa-Cure concrete curing box at a temperature of 23±2 ^{o}C and a relative humidity of 95% was utilized for curing the cubes. The cubes' compressive strength was determined using a Tinius Olsen universal compression machine with a 200,000 lb servo-controlled hydraulic pressure and paired with a computer workstation for data collection. A consistent load rate of 200 lb/sec was maintained for every test.

2.6. TGA tests

Thermogravimetric analysis (TGA) was conducted using a NETZSCH STA 449 F5 PC system. The TGA measurements were used to primarily quantify and identify the amount of free water, bound water, and other volatiles embedded into the blended cement systems. Identifying the cement phases present at various hydration times was also useful. In every test, the mass loss (thermogravimetry, TG, $\%_{mass}$) and the differential mass loss rate (DTG, $\%_{mass}$/min) were measured. The quantity of the bound water present in a sample was used to assess the degree of hydration as well as the other thermal properties of the samples. At specific ages, small pieces of the samples were extracted off from the paste specimens and submerged into the isopropanol to arrest hydration. The samples were dried in a vacuum oven for 15 min to remove any remaining solvents, ground to powder, and weighted in a consistent manner before they are placed in the TGA instrument. The loaded mass of the samples for TGA test were around 10 mg. The samples were enclosed on the alumina pan and heated from room temperature to 1000 ^{o}C with a temperature ramp of 10 ^{o}C/min under N_2 environment.

2.7. MIP tests

To determine the capillary porosity, and pore size distribution of selected 1d and 28d hydrated pastes a Mercury Intrusion Porosimeter (MIP) was utilized. The chunks of the hydrated pastes were submerged under isopropanol to arrest the hydration reaction. Before the MIP tests, the samples were dried at 70 ^{o}C for 2 days to remove the loosely attached water molecules. The temperature of 70 °C was used to effectively remove free water from the pores without significantly altering the microstructure of the cement [71,72]. However, it is noted that prolong drying at elevated temperatures of 70 °C can degrade ettringite [72], which may influence the net porosity. Although, the present porosity investigation focuses on the relative comparison of samples dried under same condition rather than the absolute porosity values. The samples were made dust free by blowing air and the dimension was maintained around 5 mm before loading into the bulb of the penetrometer. The Washburn equation [73] estimates the pore size, and the pressure needed to force mercury, a non-wetting fluid, into the cylindrical pores of the samples. The surface tension of mercury and contact angle between mercury and sample were selected as 480 erg/cm^2 and 130°. The sample preparation procedure and other testing parameter selection were followed by the guidelines on mercury intrusion porosimetry in concrete systems [74]. In this study, the mercury intrusion porosimetry (MIP) test was conducted using a Quantachrome PoreMaster (automated mercury intrusion porosimeter). First, in the low-pressure test, the mercury was filled

up into the penetrometer and made contact with the sample. Secondly, in the high-pressure tests, the mercury penetrated the pores of the samples. The measurable pores are in the range 7 nm - 0.4 mm. The final pressure of 30000 psi was employed in the MIP tests. Though for cement-related materials, because of the ink-bottle effect, the MIP method is not highly reliable, it is useful for reasonable analysis, especially for comparison purposes [75,76].

3. Results and discussions

3.1. Effect of LDH on CSA cement rheology and workability

The effect of CaAl-NO_3 LDH on CSA cement rheology is discussed in this section. To better understand the flow behavior, the rheology was studied utilizing both the static and dynamic yield stress evolution (dynamic is presented in section 3.3). **Fig. 4a** shows the evolution of time-dependent static yield stress of the LDH-dosed CSA cement pastes containing a fixed 0.1% PCE and 2 % CA (admixture utilized for dispersion and retardation, respectively), but varying dosage of LDH seeds from 1-to-5%. As seen in **Fig 4a**, the flow curve shifts to the left with increasing dosage of LDH indicating accelerated hydration and hardening with increase in LDH content. The corresponding workability parameters, obtained from this flow curves as described in section 2.3, are presented in **Fig. 4 (b-f),** showing the effect of LDH. The error bars are the standard deviation of triplicate measurements. From **Fig. 4,** it is obvious that, overall, LDH increases the flowability loss rate, , hardening rate, and acceleration angle, whereas LDH decreases the placement limit. This suggests that LDH somewhat accelerates the setting and hardening of cement. These occurrences can be because of the accelerated precipitation and development of new hydration products facilitated by the nucleation sites provided by the LDH particles in the cement paste pore solution environment. Thus, LDH catalyzes the nucleation and growth of crystals, and this effect is amplified with increase in the dosage of LDH (supporting results are discussed in section 3.4). In addition, it is reported that LDH adsorbs more water which can lead to the improvement of cement paste hardening and setting rate [77]. Consequently, the buildability of the cement paste is enhanced with increase in LDH dosage.

It is well known that there is a compatibility issue of PCE in hydrated CSA cement pastes, especially if the citric acid (CA) is dosed as a set retarder. Apart from the quick reacting hydrated CSA cement particles, because of the competitive adsorption, CA with higher anionic charge density become more adsorbed on the surface of the cement particles and makes the PCE less effective in interacting with the cement particles [78]. Thus, many researchers suggest using PCE in CSA cement systems is not reasonably effective [60]. Hence, we have examined the CSA system dosed with only CA as well as CSA system with concurrent dosage of CA and PCE.

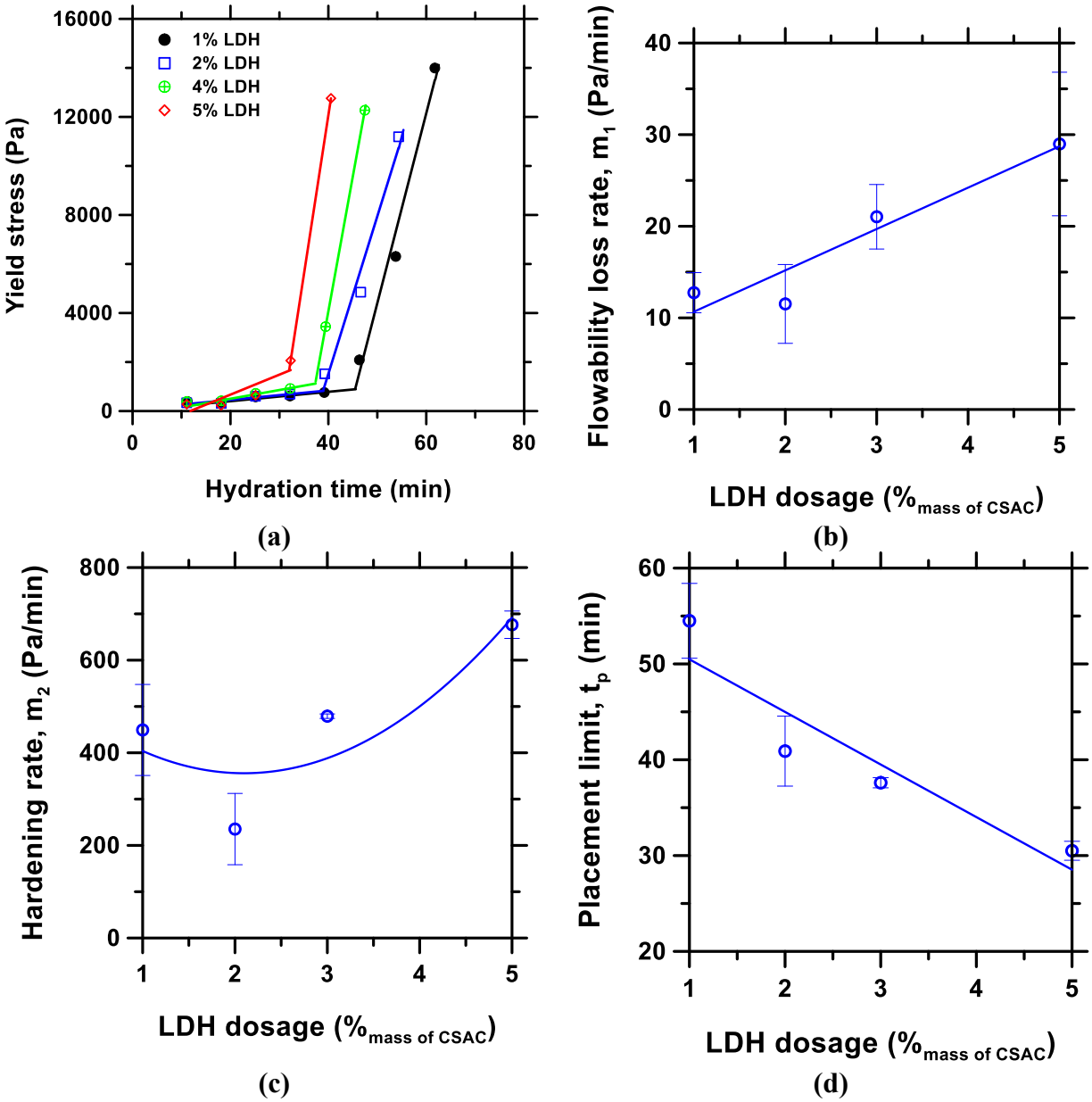
16000
12000
8000
4000
0
Yield stress (Pa)
1% LDH
2% LDH
4% LDH
5% LDH
0
20
40
60
80
Hydration time (min)
(a)
40
30
20
10
0
Flowability loss rate, m1 (Pa/min)
1
2
3
4
5
LDH dosage (%mass of CSAC)
(b)
800
600
400
200
0
Hardening rate, m2 (Pa/min)
1
2
3
4
5
LDH dosage (%mass of CSAC)
(c)
60
50
40
30
20
Placement limit, tp (min)
1
2
3
4
5
LDH dosage (%mass of CSAC)
(d)

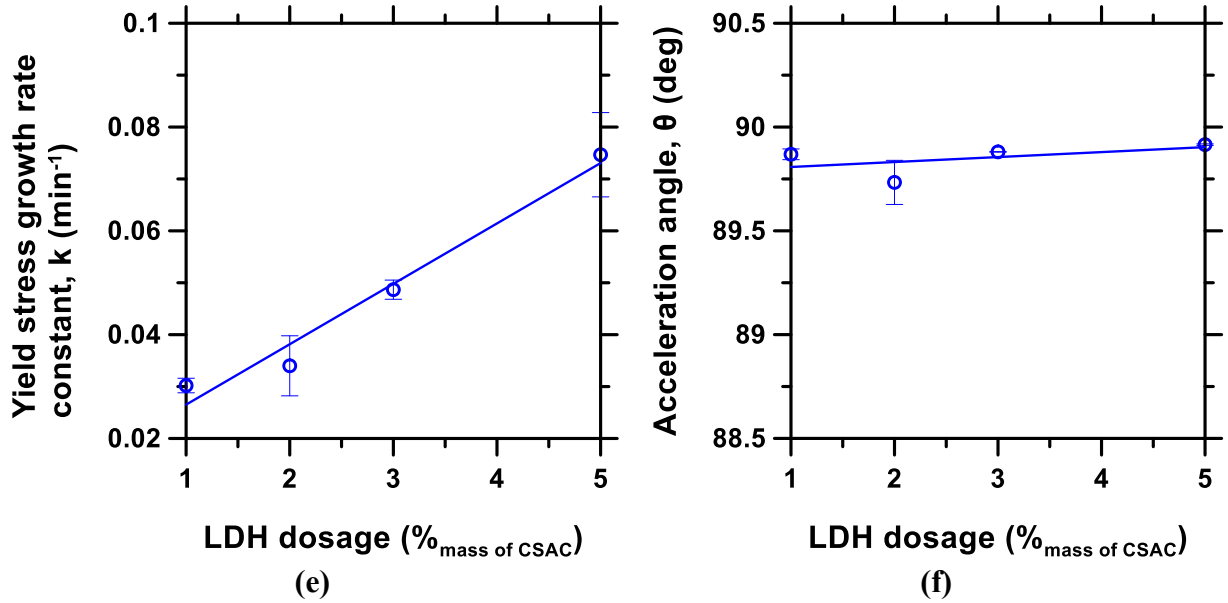

Fig. 4. Workability of CSA pastes with LDH, in the presence of 0.1% PCE: **(a)** evolution of time-dependent static yield stress in (1-5%) LDH-dosed CSA cement pastes, and **(b-f)** effect of LDH on the corresponding rheological parameters, flowability loss rate $\boldsymbol{m_1}$, hardening rate $\boldsymbol{m_2}$, placement limit $\boldsymbol{t_p}$, yield stress growth rate constant $\boldsymbol{k}$, and acceleration angle $\boldsymbol{\theta_p}$, respectively. All pastes contain a fixed 2%CA retarder.

To elucidate the effect of PCE in the CSA cement pastes, the above-presented mix design (in **Fig 4**) were studied without the incorporation of PCE, keeping all other parameters same. The results without PCE are displayed in **Fig. 5**, which provide more insights on the effect of PCE in CSA cement rheology. Comparing the results in **Fig. 4 and 5**, reveal the influence of PCE in the paste's rheology. As shown in **Fig. 6**, PCE decreases the $\boldsymbol{m_1}$, $\boldsymbol{m_2}$, $\boldsymbol{k}$, and $\boldsymbol{\theta_p}$ around 2-3 times, whereas there is almost no impact of PCE on the placement limit, $\boldsymbol{t_p}$. The results obtained for $\boldsymbol{m_1}$, $\boldsymbol{m_2}$, $\boldsymbol{k}$, and $\boldsymbol{\theta_p}$, showing a considerable effect of PCE may seems contrary to the published studies [79–81], where the findings suggest that due to the competitive adsorption of PCE with retarder, PCE will have almost no influence in the CSA pastes. However, in this study, the effect of PCE can be attributed to the slightly different working mechanism due to the presence of NO_3-LDH in the systems. The PCE can easily be intercalated into the anionic layers in the LDHs replacing the NO_3^-, and following the control release capability of LDHs [28,53,82], the PCE might be released into the cement suspension after a certain time, and making a natural impact of PCE to the systems. Thus, due to the potential intercalation in LDH and modulated release, the PCE may avoid the competitive adsorption with the higher anionic charged density-contained citrate ions, and can continue its superplasticizing effect. Using the LDH thus improve the synergistic effect and can be beneficial for some target applications, where a fixed set time is required but simultaneously controlling the hydration kinetics is anticipated (e.g., 3D printing of concrete).

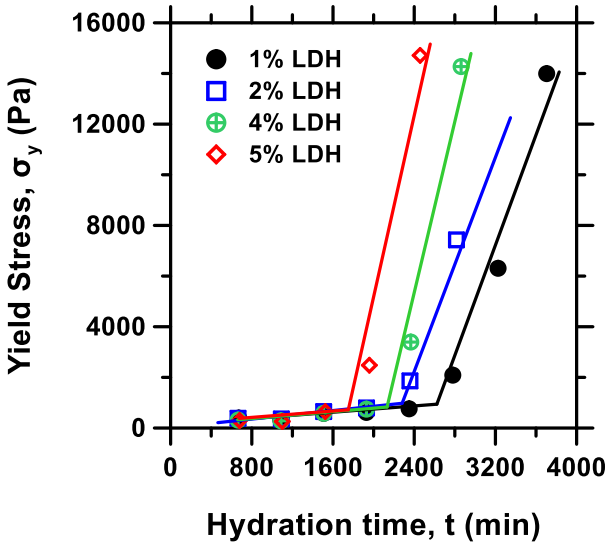
Yield Stress, σ_y (Pa)
16000
12000
8000
4000
0
0
800
1600
2400
3200
4000
Hydration time, t (min)
1% LDH
2% LDH
4% LDH
5% LDH

(a)

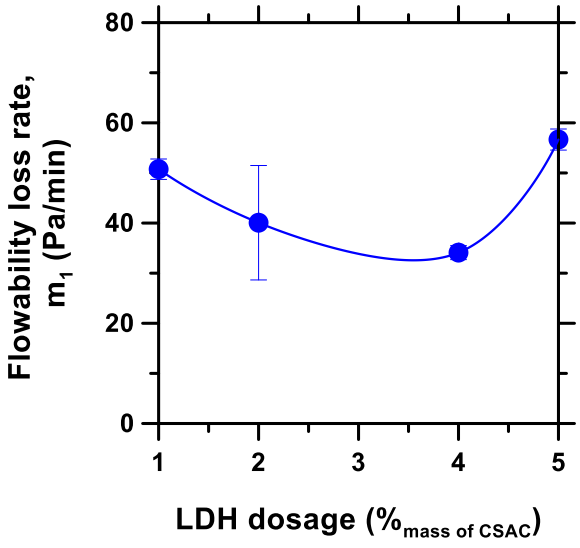
Flowability loss rate, m_1 (Pa/min)
80
60
40
20
0
1
2
3
4
5
LDH dosage (%mass of CSAC)

(b)

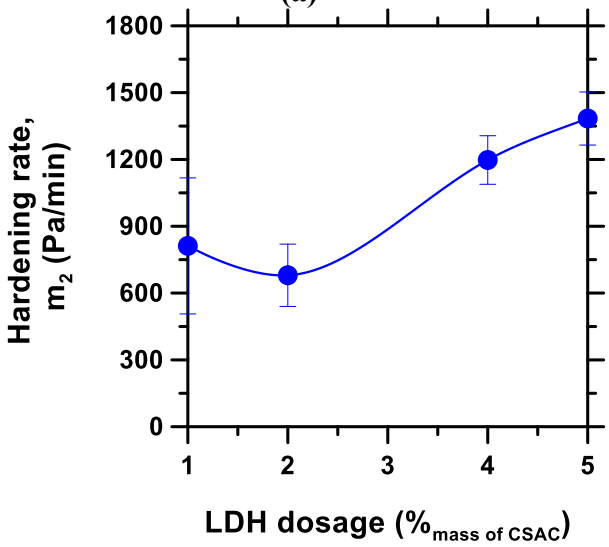
Hardening rate, m_2 (Pa/min)
1800
1500
1200
900
600
300
0
1
2
3
4
5
LDH dosage (%mass of CSAC)

(c)

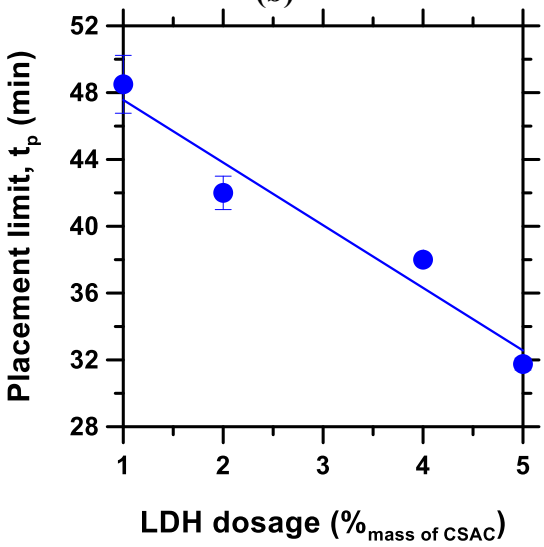
Placement limit, t_p (min)
52
48
44
40
36
32
28
1
2
3
4
5
LDH dosage (%mass of CSAC)

(d)

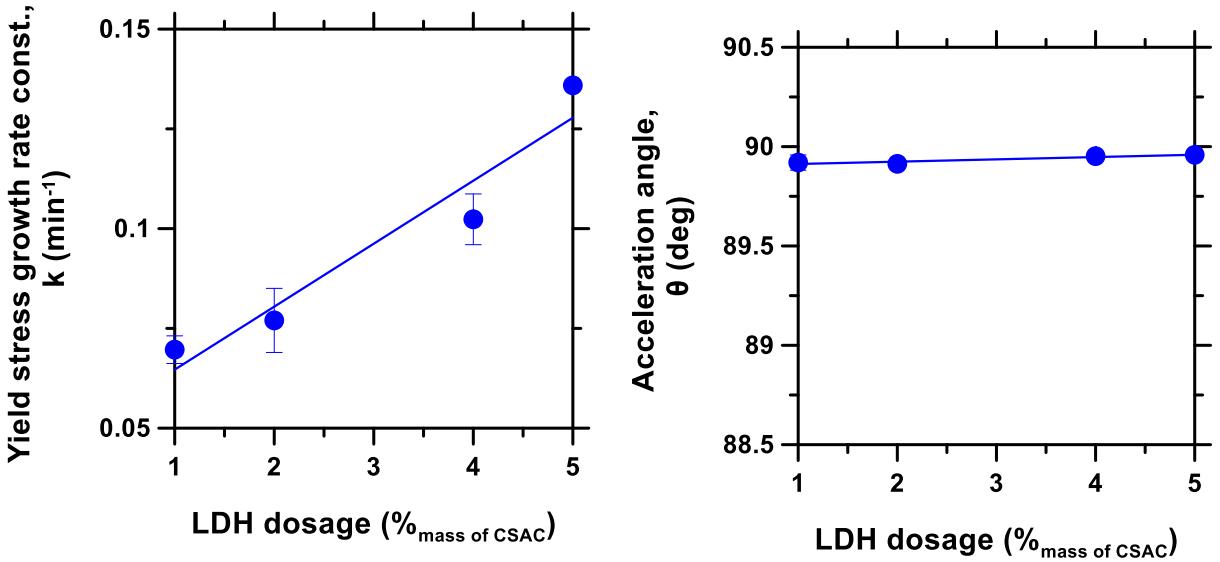

(e) **(f)**

Fig. 5. Workability of CSA cement pastes in the absence of PCE; **(a)** evolution of time-dependent static yield stress in (1-5%) LDH-dosed CSA cement pastes, and **(b-f)** effect of LDH on the corresponding rheological parameters, flowability loss rate $\boldsymbol{m_1}$, hardening rate $\boldsymbol{m_2}$, placement limit $\boldsymbol{t_p}$, yield stress growth rate constant $\boldsymbol{k}$, and acceleration angle $\boldsymbol{\theta_p}$, respectively. All pastes contain a fixed 2%CA retarder.

328

329

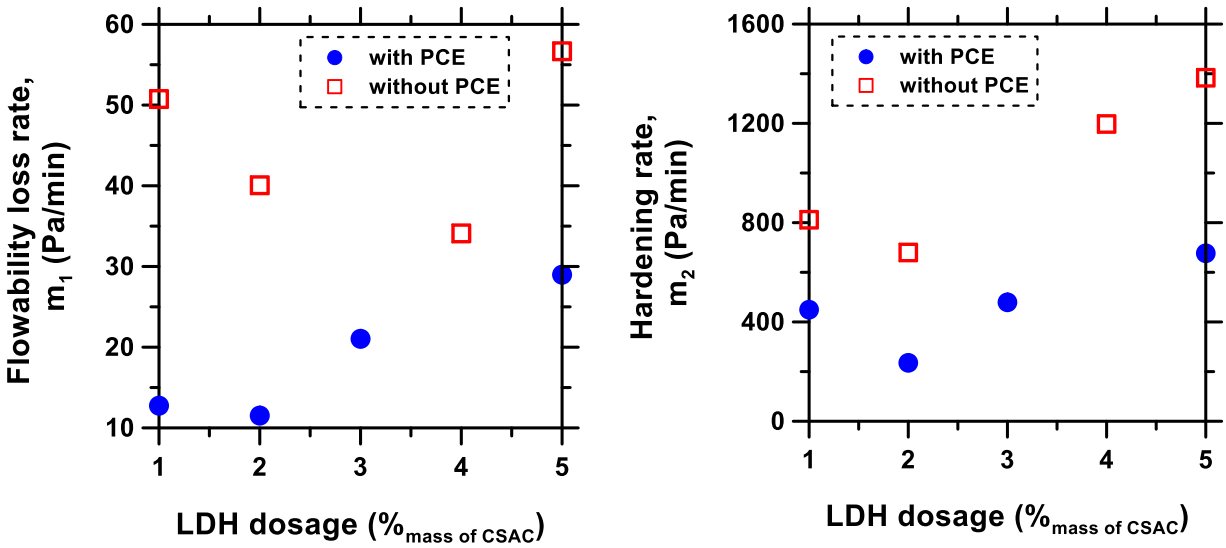

(a) **(b)**

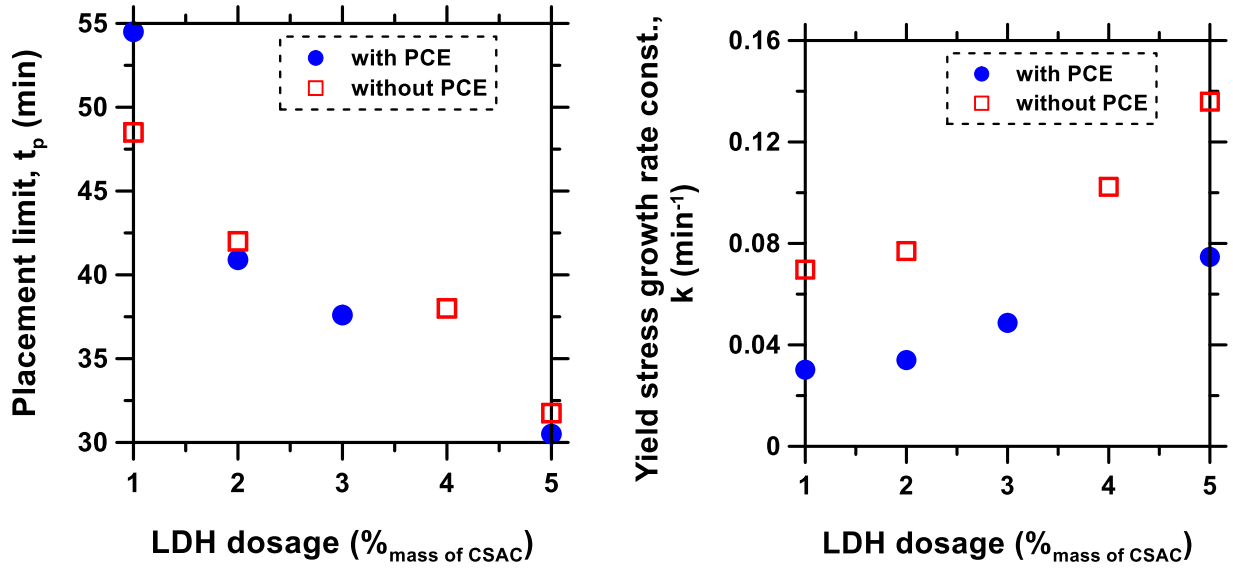

Fig. 6. Effect of PCE in CSA cement systems.

330

331 ***3.2. Effect of LDH on OPC paste rheology.***

332 The effect of (1-5%) dosages of CaAl-NO_3 LDH on OPC pastes rheology is also studied to get
333 more insights of influence of LDH in different cement pastes. In this study, all the OPC pastes
334 were prepared with 0.1% PCE as dispersant. Similar to CSA cement systems, LDH increases the
335 flowability loss rate ($\boldsymbol{m_1}$), hardening rate ($\boldsymbol{m_2}$), yield stress growth rate constant ($\boldsymbol{k}$), and
336 acceleration angle ($\boldsymbol{\theta_p}$), and decreases the placement limit ($\boldsymbol{t_p}$) (**Fig. 7**). As stated above, LDH can
337 act as a seeding or stiffening agent in the cement systems, accelerating nucleation kinetics and
338 growth of the hydrated cement phases, thereby increasing the buildability of the cement pastes.

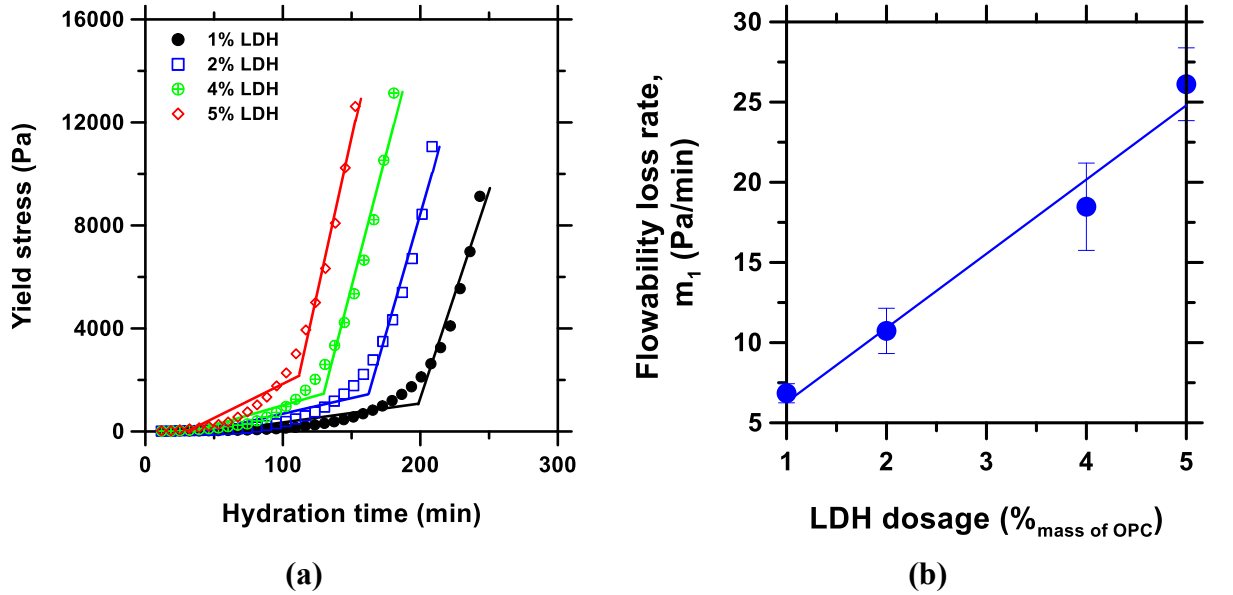

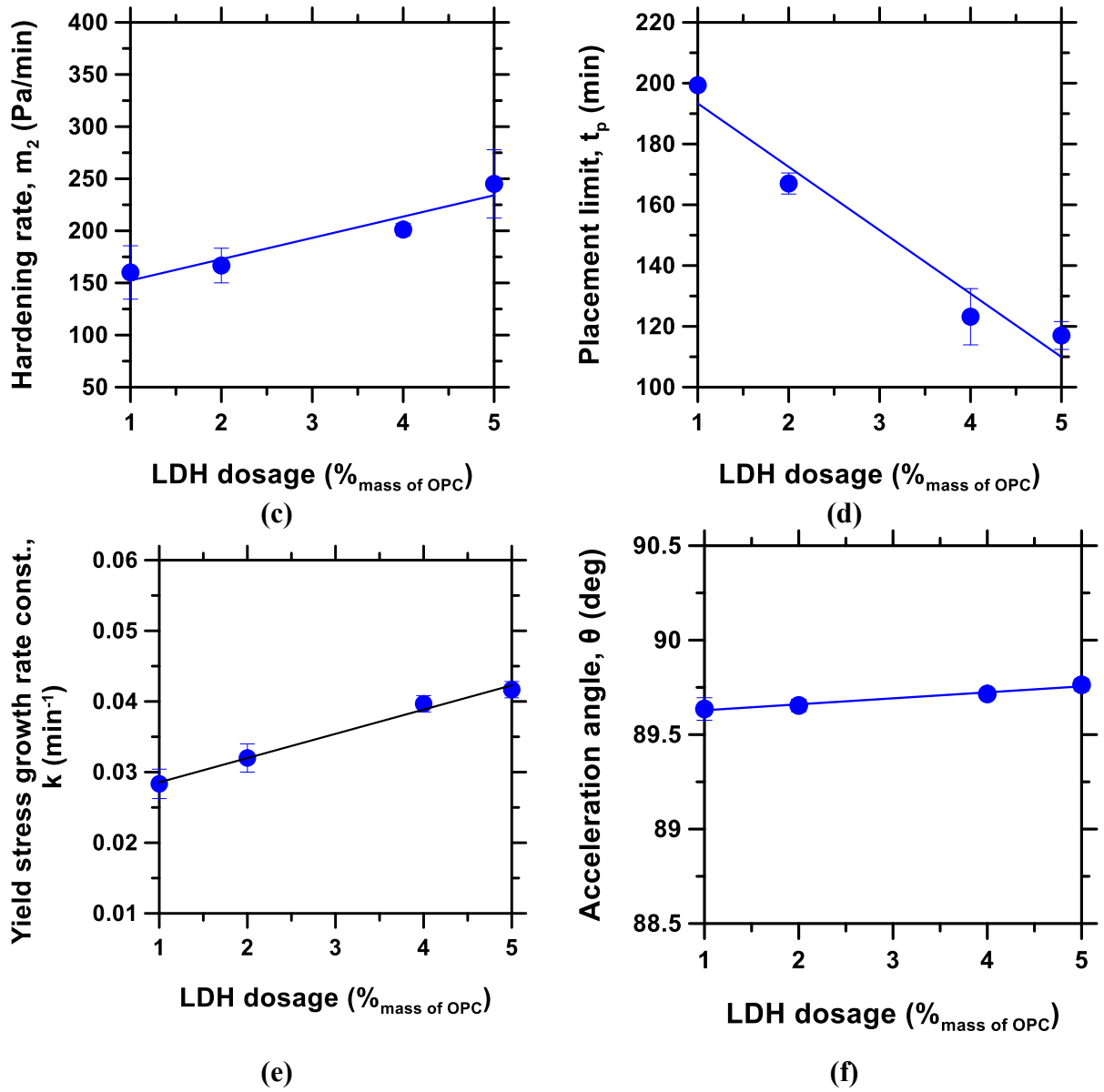

Fig. 7. Workability of OPC pastes: **(a)** evolution of time-dependent static yield stress in (1-5%) LDH-dosed OPC pastes, and **(b-f)** effect of LDH on the corresponding rheological parameters, flowability loss rate $\boldsymbol{m_1}$, hardening rate $\boldsymbol{m_2}$, placement limit $\boldsymbol{t_p}$, yield stress growth rate constant $\boldsymbol{k}$, and acceleration angle $\boldsymbol{\theta_p}$, respectively.

3.3. Effect of LDH on dynamic rheology of cement pastes

In order to gain more insights of the rheological properties, different methods of yield stress evolution were studied. Both static and dynamic yield stresses hold significance for numerous practical applications [83]. For instance, understanding the static yield stress of cement pastes can provide insights into their stability and resistance to deformation from rest. On the other hand, the dynamic yield stress offers valuable data regarding the flow behavior of cement when it's pumped and during the extrusion process in 3D printing of concrete. Thus, dynamic yield stress of cement

pastes under the influence of PCE has frequently been researched in cement field to understand pumping and bleeding [84]. The dynamic yield stresses of cement pastes is preferred to be small for pumping, whereas the static yield stresses are preferred high for better stability and lesser formwork pressure [85,86]. The evolution of dynamic yield stress and plastic viscosity of the CSAC and OPC cement pastes (CSA + 1-5% LDH+ 0.1 % PCE + 2 % CA [w/c = 0.5]) and (OPC + 1-5% LDH + 0.1% PCE [w/c = 0.5]), and the corresponding rheological parameters are presented in **Fig. 8 and 9**, respectively. In the test method, a conditioning step was always followed by a ramp-up and ramp-down steps. The ramp-down steps were executed after a 5 s rest following the ramp-up. The traditional Bingham model was employed to determine the dynamic yield stresses and plastic viscosities, $\boldsymbol{\sigma^* = \sigma_y + \dot{\gamma}.\mu_{pl}}$; where $\boldsymbol{\sigma^*}$ (variable) is the dynamic shear stress in a step, $\boldsymbol{\sigma_y}$ is the dynamic yield stress, $\boldsymbol{\dot{\gamma}}$ is the shear rate ranging from 0 - 200 s^{-1}, and μ_{pl} is the plastic viscosity. As stated above, compared to the static yield stresses, dynamic yield stresses are lower, and simultaneously the placement limits are extended. The static yield stress values and the stress overshoot magnitude can be significantly impacted by the rest interval between the end of the pre-shear and the test run [87].

In this section three most important workability parameters, $\boldsymbol{m_1}$, $\boldsymbol{m_2}$, and $\boldsymbol{t_p}$ were analyzed, and the trends for both cement pastes are similar to the trends obtained utilizing static yield stress, presented in earlier sections. However, the magnitudes are significantly lower for, $\boldsymbol{m_1}$ and $\boldsymbol{m_2}$ in the dynamic tests compared to the static tests, because the up-ramp flow and shear history of the dynamic test methods breaks the structure and bonding in the hydrated cement pastes prior to the down-ramp used in obtaining the dynamic yield stress and plastic viscosity data. For the same shear history difference and perturbation of hydration process, the $\boldsymbol{t_p}$ parameter is higher in the dynamic than in the static yield stress method.

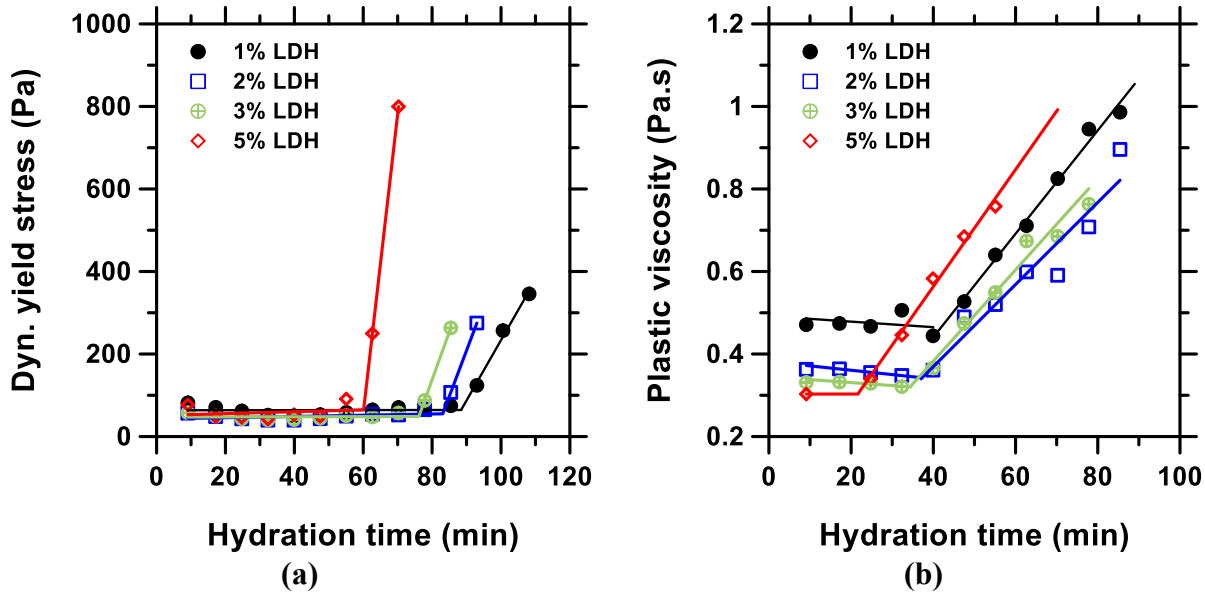

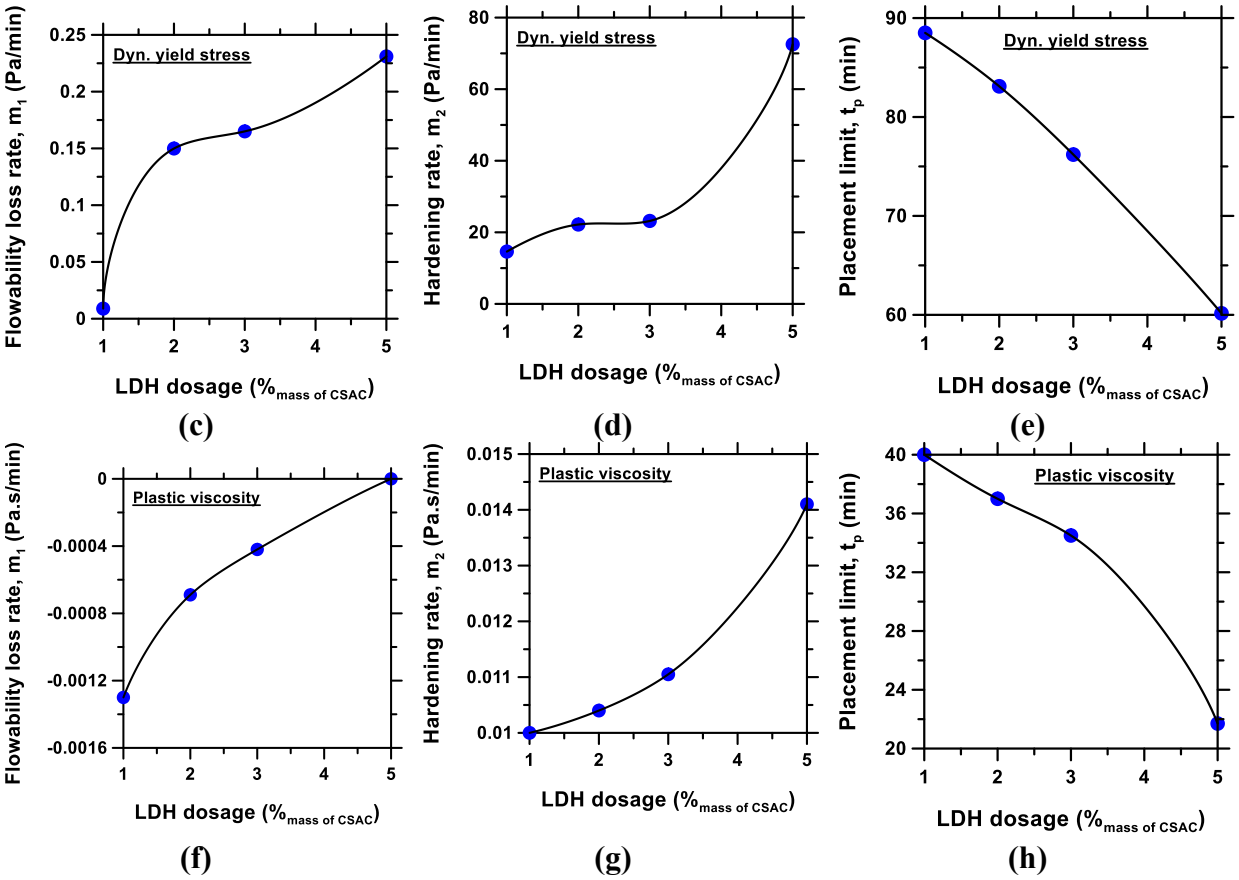

Fig. 8. Workability of CSAC pastes derived from dynamic tests: **(a)** time-dependent evolution of dynamic yield stress, and **(b)** development of plastic viscosity, **(c - e)** evolution of rheological parameters from the dynamic yield stress method, and **(f - h)** evolution of rheological parameters in utilizing the plastic viscosity data.

372

373

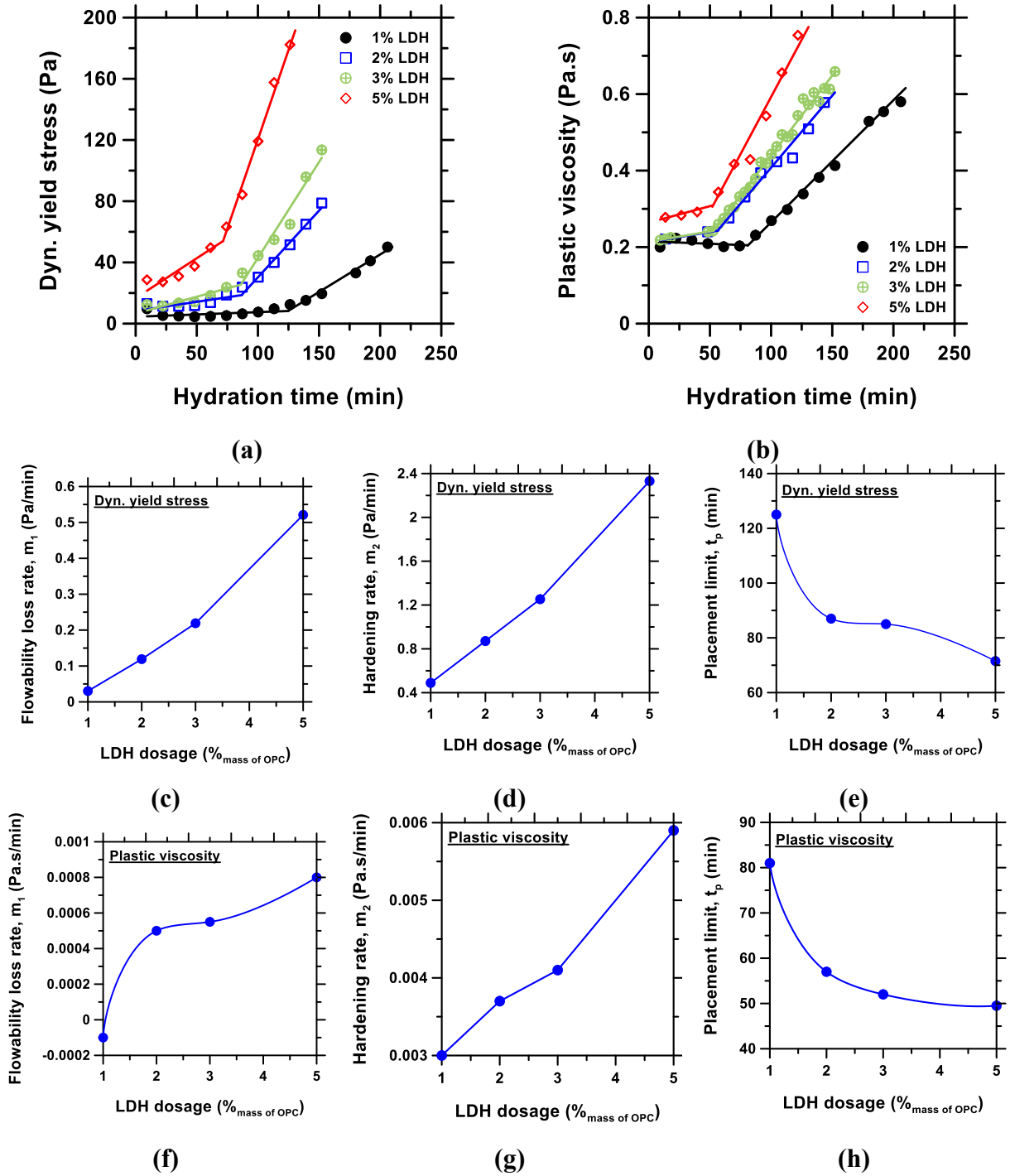

Fig. 9. Workability of OPC pastes derived from dynamic tests: **(a)** time-dependent dynamic yield stress evolution, and **(b)** development of plastic viscosity, **(c - e)** evolution of rheological parameters from the dynamic yield stress method, and **(f - h)** evolution of rheological parameters utilizing the plastic viscosity data.

3.4. Effects of LDH on the evolution of cement hydrate phases

The effect of the LDH on the hydrated phase assemblage was tracked as a function of time, by examining the XRD pattern of the pastes seeded with 5%LDH in comparison with the control (0%LDH) at multiple intervals, for up to 28days. **Fig. 10** shows the evolution of hydrated cement phases over time. From **Fig. 10 (a)** and **(b),** it is evident that the ettringite peaks grew faster in the LDH-dosed OPC pastes compared to the control, as can been seen on the 3h diffraction patterns. Also, the gypsum peaks diminished faster in the LDH-dosed OPC pastes compared to the control. This observation indicates that the addition of LDH accelerated the precipitation of ettringite and concurrently led to faster consumption of gypsum compared to the control paste at early age. Conversely, at the later age of 28days (**Fig. 10e**), it is difficult to distinguish the phase assemblage of LDH-seeded OPC paste from the control, indicating that the effect of LDH is more significant at the early age stages than the later age. Similar trend was obtained with CSAC pastes, where ettringite grew faster as seen in the 1h data of the LDH-dosed CSAC pastes compared to the control (**Fig. 10 (c) and (d)**), and at later age the system equilibrated featuring identical phase assemblage (**Fig. 10f**). These results clearly agree with the fresh paste rheology that suggesting that the LDH seeds provides nucleation sites that encouraged rapid formation and growth of new hydration products at early age resulting in the accelerated stiffening and hardening of the pastes with LDH dosage.

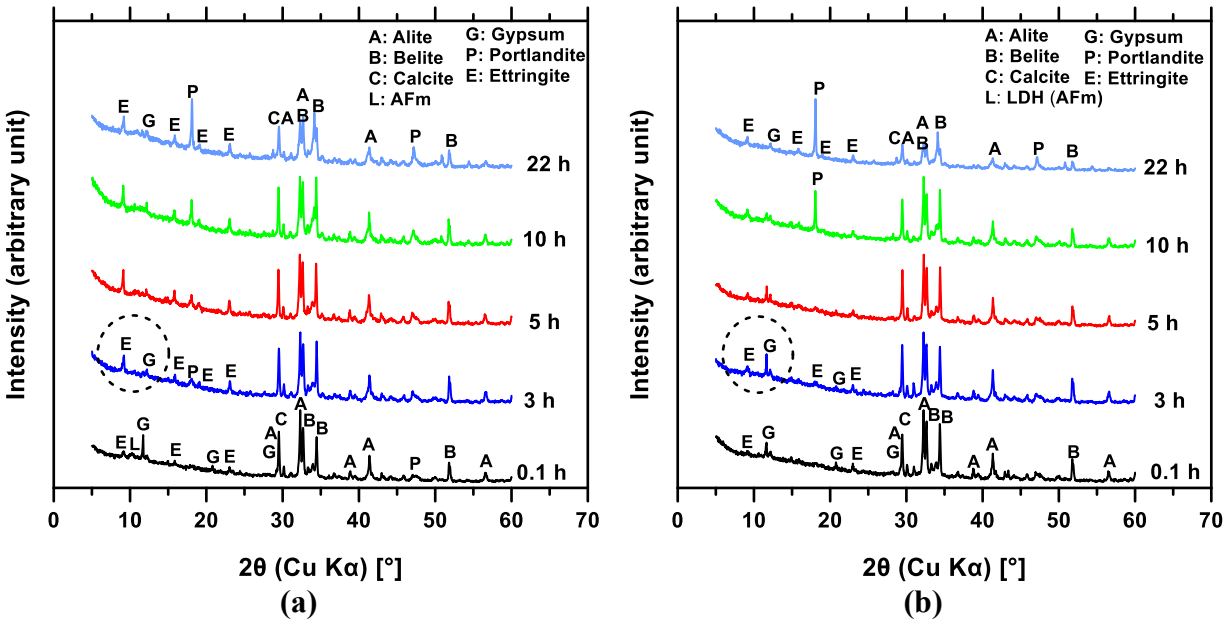

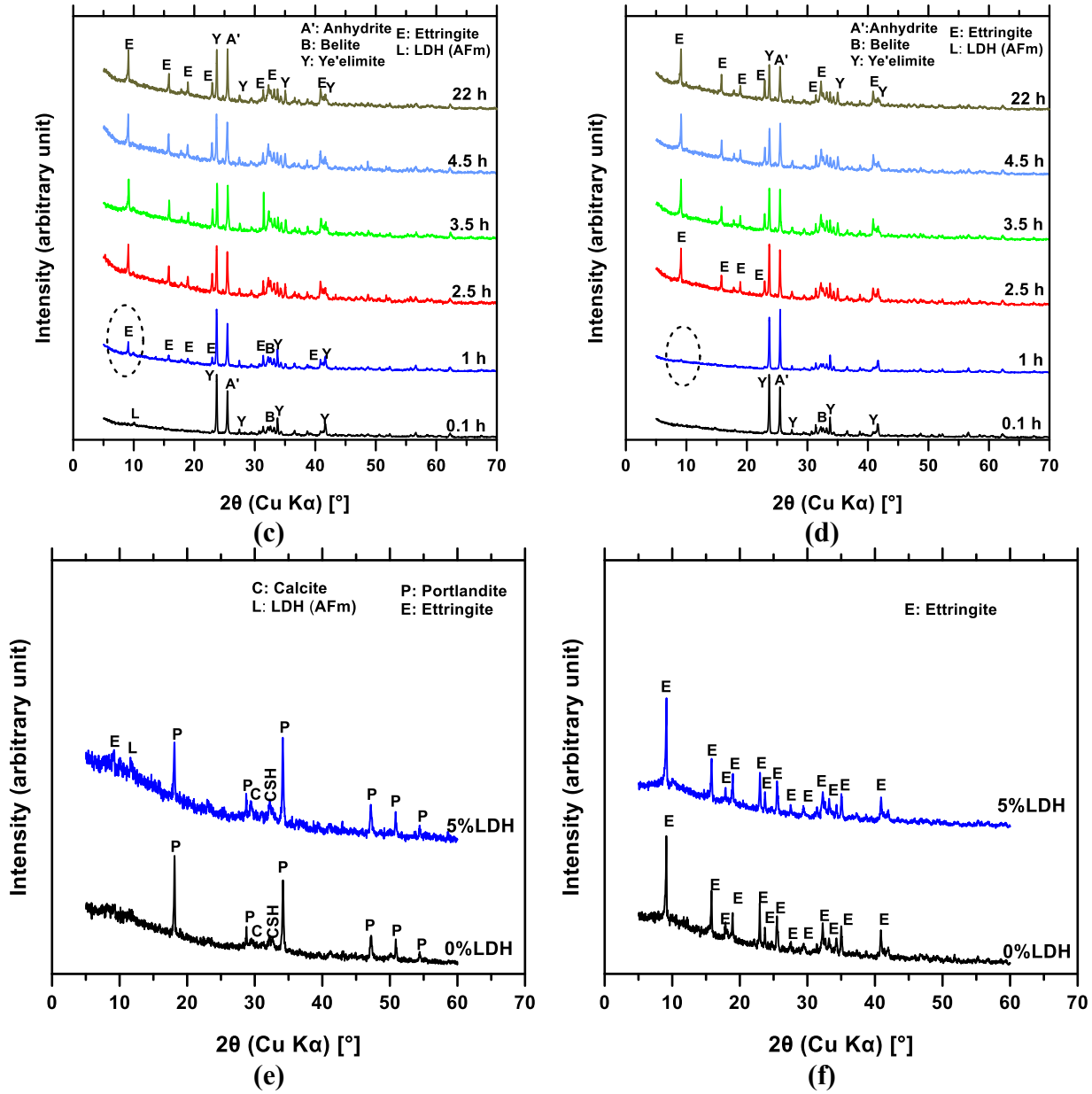

Fig. 10. Evolution of hydrated cement phases over time: **(a)** OPC+5% LDH, **(b)** OPC+0% LDH (control), **(c)** CSA+5% LDH, and **(d)** CSA+0% LDH (control), **(e)** 28 day OPC pastes, **(f)** 28day CSAC pastes.

3.5. Isothermal calorimetry

The results from the isothermal calorimetric analyses of CSA cement and OPC pastes seeded with 0-5%LDH are shown in **Fig 11**. The aim of the isothermal calorimetry was to (i) identify attributes that could be linked to the rheological properties of the pastes, (ii) to know their heat evolution profiles at an early-age, and (iii) the effect of LDH dosage on the calorimetry profiles of the CSA cement and OPC systems. **Fig. 11(a) and (b)** presents the heat flow and cumulative heat profiles of the CSAC pastes over a 24-hour curing time. It is observed that with increase in LDH content,

heat flow increases at both the induction and acceleration stages, with a noticeable shift of the heat flow peak to the left (**Fig. 10(a)**) and rise in the cumulative heat over 24 h (**Fig. 10(b**)). These characteristics indicates acceleration of the CSA cement hydration with LDH dosage, in agreement with the rheology and mineral phase assemblage tracking, all of which supports the postulate that LDH provides additional surfaces with crystal nuclei in the suspension thereby accelerating nucleation and growth of hydrates, as has been observed for other type of LDHs [88,89]. The cumulative heat generation is expectedly higher in 5% LDH-dosed system, compared to the one with 0% LDH dose. The CSA systems follows the trend of increased heat evolution as the dosing 5% > 4% > 3% > 2% > 1% LDH. This effect observed in isothermal calorimetry is similar to the rheological studies; more LDH-induced hydrated products increased the loss of flowability ($\boldsymbol{m_1}$), increased the hardening rate ($\boldsymbol{m_2}$), growth rate constant ($\boldsymbol{k}$), and decreased the placement limit ($\boldsymbol{t_p}$).

Compared to CSA systems, OPC pastes show a more noticeable shift of the peak heat flow to the left which signifies a shrinking of the dormant period and acceleration of hydration (**Fig 11(c) and 9(d)),** which agrees with the rheology and phase assemblage data**.** However, the peak heat flow and 24-hour cumulative heat are observed to decrease with LDH dosage, in contrast with the trend with CSA pastes. The observed decrease in cumulative heat of the OPC pastes with increase in LDH dosage, despite the increase in hydration kinetics, is a new finding that can be explained as follows. First, the LDH seed in the cement systems provides nucleation sites for formation of new LDH nuclei which subsequently converts almost immediately or slowly to ettringite depending on the sulfate concentration of the pore solution according to **Eq. (1).** It is therefore expected that the conversion of the new nuclei to ettringite is almost instant in CSA cement pastes due to the supersulfated pore solution at early age leading to a chemical reaction dominated by **Eq (2)** with high heat of formation. Hence the heat release is increased for the CSA cement paste containing LDH seeds. Conversely, in OPC systems with moderate sulfate concentration and high calcium ion concentration at early age, it is expected that the new LDH nuclei formed will convert to ettringite more slowly than it is formed leading to a reaction that is dominated by **Eqs (3) and (4)** with lesser heat release than **Eq 1** pathway, which may be contributory to the lower overall heat release in the OPC systems with LDH seeding within the first 24 hours of hydration.

$$C_4AsH_{12}(AFm) \xleftrightarrow[\pm\, 2(Ca^{2+}+SO_4^{2-});\, 20H]{} C_6As_3H_{32}\ (AFt) \quad (1)$$

$$6Ca^{2+} + 2Al(OH)_4^- + 3SO_4^{2-} + 4OH^- + 26H_2O \rightarrow Ca_6Al_2(SO_4)_3(OH)_{12}\cdot 2\,6H_2O : \Delta fH° = -17{,}535\ kJ/mol \quad (2)$$

$$4Ca^{2+} + 2Al(OH)_4^- + SO_4^{2-} + 4OH^- + 6H_2O \rightarrow Ca_4Al_2(SO_4)(OH)_{12}\cdot 6H_2O : \Delta fH° = -8{,}758.6\ kJ/mol \quad (3)$$

$$4Ca^{2+} + 2\,Al(OH)_4^- + 2\,NO_3^- + 4OH^- + 4H_2O \rightarrow Ca_4Al_2(OH)_{12}(NO_3)_2\cdot 4H_2O : \Delta fH° = -7{,}719.3\ kJ/mol \quad (4)$$

Additionally, a closer look at the phase assemblage shown in **Fig. 10(a) and (b)** reveals more calcite formation in LDH-dosed OPC systems, and calcite formation is an endothermic process that can lead to lower heat generation.

Thus, LDH-OPC composites with accelerated hardening but lower heat generation can be beneficial for certain applications, including 3D printing, where a less heat generation is desired (for preventing crack formations, maintaining better microstructural stability, and other benefits), and higher buildability with accelerated hardening is critically expected. The calorimetry data for OPC agrees with the 1d TGA data presented in the latter section, i.e., addition of LDH contributed to accelerated reaction (more bound water).

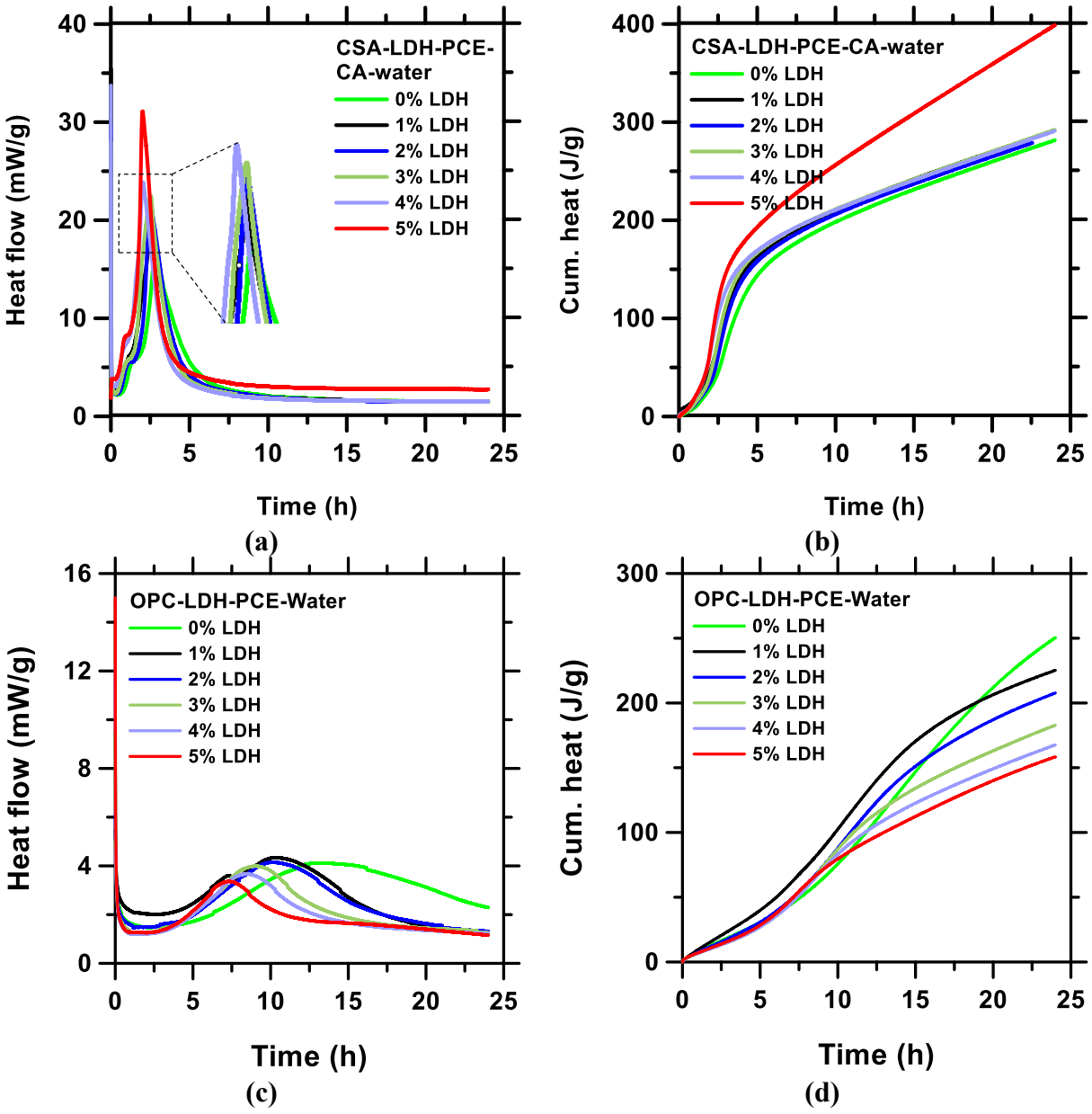

Fig. 11. Isothermal micro reaction calorimetry revealed the time-dependent: **(a)** heat flow from [CSAC+LDH] pastes, **(b)** cumulative heat from [CSAC+LDH] pastes, **(c)** heat flow from [OPC+LDH] pastes, **(d)** cumulative heat from [OPC+LDH] pastes. All the pastes were prepared with 0.1% PCE at w/c = 0.5, additionally 2% CA was used in CSA cement pastes.

3.7. Thermal analysis

The thermogravimetric analysis (TGA) and differential thermogravimetry (DTG) curves of 0% and 1% CaAl-NO_3 LDH-dosed 1d and 28d OPC and CSA cement samples are shown in **Fig. 12**. The mass losses (%) of the samples at different temperature ranges are presented in **Table 3**. Typically, the free or evaporable water is eliminated within 0 - 110 ºC [92], decomposition and loss of loosely bound water in gypsum, ettringite, C-S-H and other hydrated phases including LDH happens in 110 - 170 ºC [92–95], decomposition of C-S-H, LDH and loss of the remaining bound water occurs in 170 - 300 ºC [92,96,97], dihydroxylation of portlandites occur within 450 – 550 ºC [92,93], and decarbonation and losses of other volatiles happens at ≥ 600 ºC [92,98]. It is worth noting that C-S-H gel decomposes around similar temperature as ettringite making it difficult to differentiate the mass loses due to C-S-H and ettringite. However, this study mainly focused on the losses of free water (unbound water), bound water, and other volatiles. Free water losses were counted to 110 ºC, bound water from 110 – 600 ºC, and volatiles from 600 – 1000 ºC. The bound water content is related to the degree of hydration of the individual samples and can be proportionately related to the heat evolution in the calorimetry as well as to compressive strength development of the samples. For example, the bound water content in 1d LDH-dosed OPC and CSA samples are higher than the control samples. This is attributable to the accelerated hydration reaction by LDH as seen in calorimetry results where the heat flow peaks shifted to the left. The bound water content in LDH-dosed samples at 28d is comparatively lower than their respective control samples, which can be associated with lower degree of hydration at later ages suggesting that the effect of LDH is much more beneficial at early age. However, the total mass loss still shows higher amounts for the LDH-dosed pastes at 28 days, and a close look also reveals significantly higher mass loss for the LDH-dosed pastes below 110 ºC compared to the control (**Table 3**). It has been reported that ettringite may begin to decompose and release its water from temperature as low as 50 ºC[94,99,100] which may suggest underestimated bound water, especially for the CSA system.

Also, the higher mass loss below 110 ºC LDH-dosed pastes cured for 28 days compared to the controls may suggest that the addition of LDH impacts a hygroscopic-like property to the pastes at later stage, encouraging the entrapment of unreacted or loose water molecules in the metrices, which lead to lower compressive strength. **Figure 13** depicts the structure of LDH with the interlayer anions. When external anions (e.g., OH^-) are introduced to the environment, LDH has the capability to trap these anions, a process that simultaneously involves the displacement and release of anions initially situated in the interlayer spaces. The nitrate ions (NO_3^-) present in the LDH, may easily get exchanged with the OH^- or water molecules. Thus, the entrapped water molecules in the LDH particles may not actively participate in the hydration reaction, which can be responsible for more incomplete reaction and or overall higher disposable water content, leading to less strength development. The possible mechanism of exchanged anions and encapsulation of water or hydroxyl molecules are presented in **Fig. 13**.

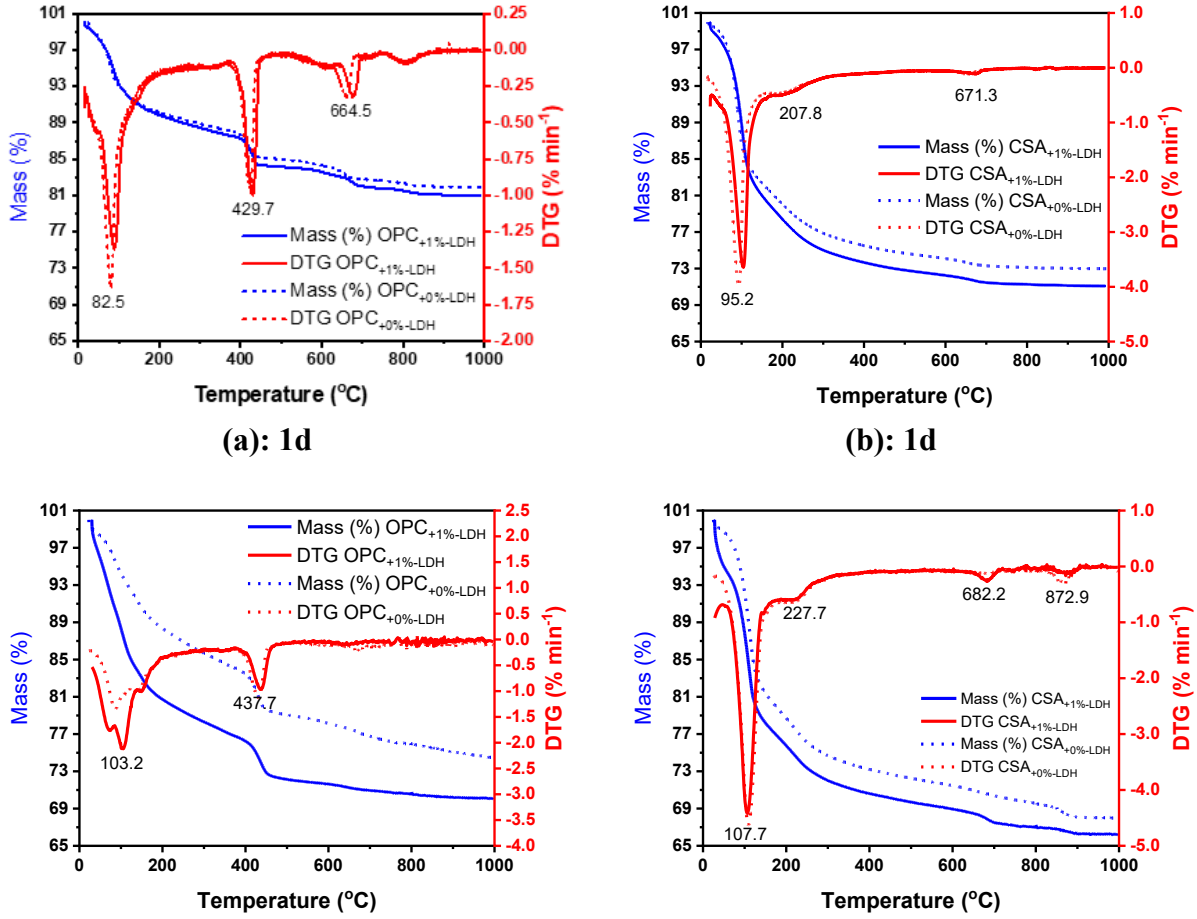

Fig. 12: Thermal analysis of 1d and 28d control and 1% LDH-dosed **(a, c)** OPC, and **(b, d)** CSA cement samples. All the samples were prepared with the same designed mix proportions.

491

492

Table 3. TGA of blended cement samples

Materials (with admixtures)	**Mass (%) losses of 1d and 28d OPC samples**			**Total mass loss (%)**
	≤ 110 °C (free water)	110 – 600 °C (bound water)	600 – 1000 °C (other volatiles)	
OPC + 0%LDH- 1d	7.48	8.24	2.36	18.08
OPC + 1%LDH- 1d	7.40	9.02	2.59	19.01
OPC + 0%LDH- 28d	6.59	15.27	3.72	25.58
OPC + 1%LDH -28d	13.28	15.09	1.57	29.94
	Mass (%) losses of 1d and 28d CSAC samples			
CSA + 0%LDH- 1d	14.99	10.93	1.10	27.02
CSA + 1%LDH- 1d	14.84	12.91	1.16	28.92
CSA + 0%LDH- 28d	11.35	17.2	3.52	32.07
CSA + 1%LDH- 28d	15.74	15.32	2.73	33.79

493

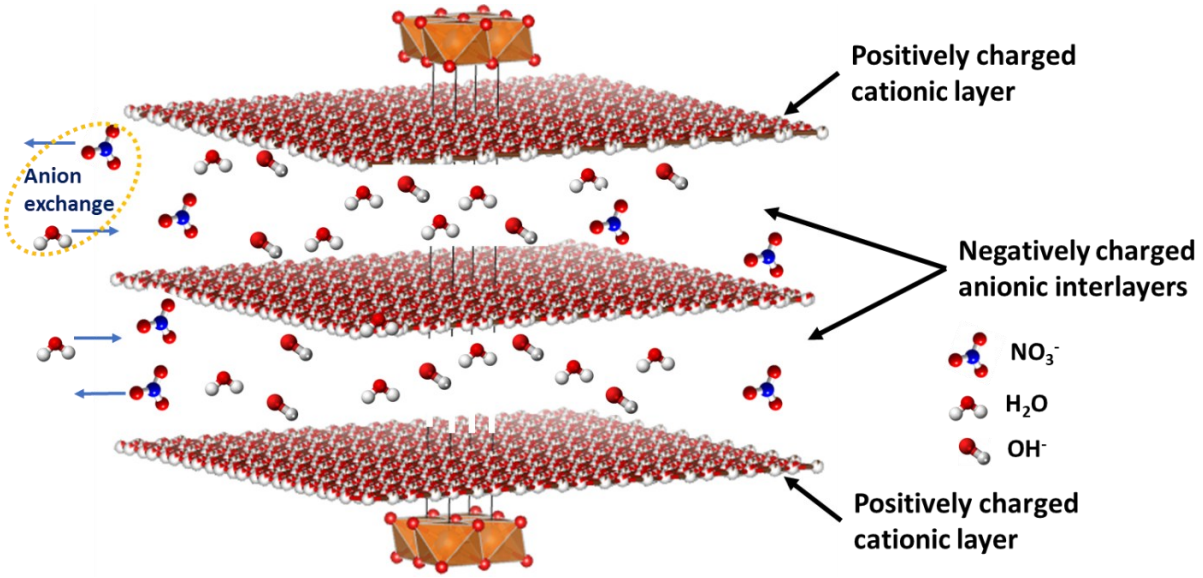

Fig. 13. Illustration of entrapped and loosely attached unbound water molecules into the CaAl-NO_3 LDH layers, and exchange of nitrate ions with water or hydroxyl molecules present in the pore solution in the cement systems.

494

495 ***3.7. Mercury intrusion porosimetry***

496 The porosity and pore size distribution of 0% and 1% LDH-dosed cement samples obtained by
497 mercury intrusion porosimetry (MIP) is shown in **Fig. 14** and **Fig. 15**. The overall porosity of the
498 samples is summarized in **Table 4**. **Figure 14** shows the porosity and pore size distribution of 1d
499 and 28d OPC samples. The porosity of the 1d OPC samples are nearly the same (**Fig. 14(a)**).
500 However, **Fig. 14 (c, d, g, h)** shows that there are larger pores in the 1% LDH-dosed sample, which
501 can be responsible for the slightly reduced compressive strength of 1% LDH-dosed OPC sample.
502 **Fig. 14 (e, f, g)** indicates that the LDH-dosed OPC sample cured for 28 days feature higher porosity
503 and larger pores, which similarly corroborate the reduced compressive strength found for the 28d
504 LDH-dosed sample, compared to control. An almost similar pattern can be observed for the CSA
505 cement systems in **Fig. 15**. LDH-dosed CSA samples displayed nearly the same overall porosity;
506 however the LDH-dosed samples had more pores with larger volumes. The nature of the porosity
507 profiles were found similar to the published work [101–104]. Higher porosity and especially larger
508 pores decreased the mechanical strength of most of the LDH-dosed pastes, albeit the decrease in
509 strength is very negligible in the CSAC pastes (**section 3.8**). Thus, the incorporation of CaAl-NO_3
510 LDH in this study showed no improvement in the strength development of the blended cement
511 samples. Reducing the size of the LDH, for example, submicron-to-nano LDH, and utilizing lower
512 amount of dosage (e.g., < 1%) and more robust particle dispersion protocol may be suggested for
513 future investigations. As stated in section 2.7, it is possible for some ettringite to degrade during
514 the drying which may have affected the absolute porosity, especially for the CSAC samples.
515 However, since the control samples were dried under the same conditions as the LDH-modified
516 samples, the comparison of the results relative to each other can still provide useful information
517 despite any errors potentially arising from the drying protocol.
518

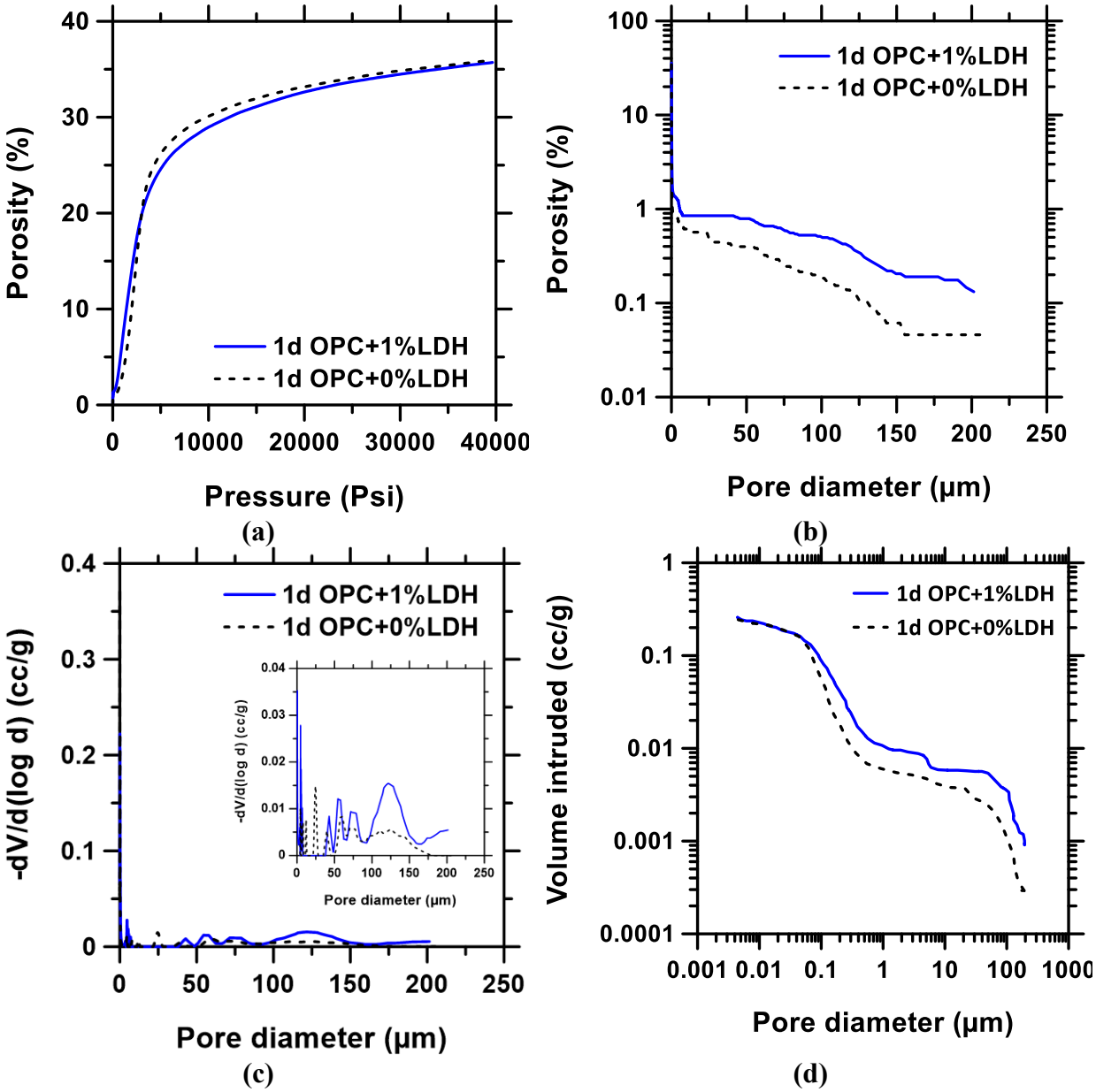
Porosity (%)
Pressure (Psi)
1d OPC+1%LDH
1d OPC+0%LDH
(a)
Porosity (%)
Pore diameter (μm)
1d OPC+1%LDH
1d OPC+0%LDH
(b)
-dV/d(log d) (cc/g)
Pore diameter (μm)
1d OPC+1%LDH
1d OPC+0%LDH
(c)
Volume intruded (cc/g)
Pore diameter (μm)
1d OPC+1%LDH
1d OPC+0%LDH
(d)

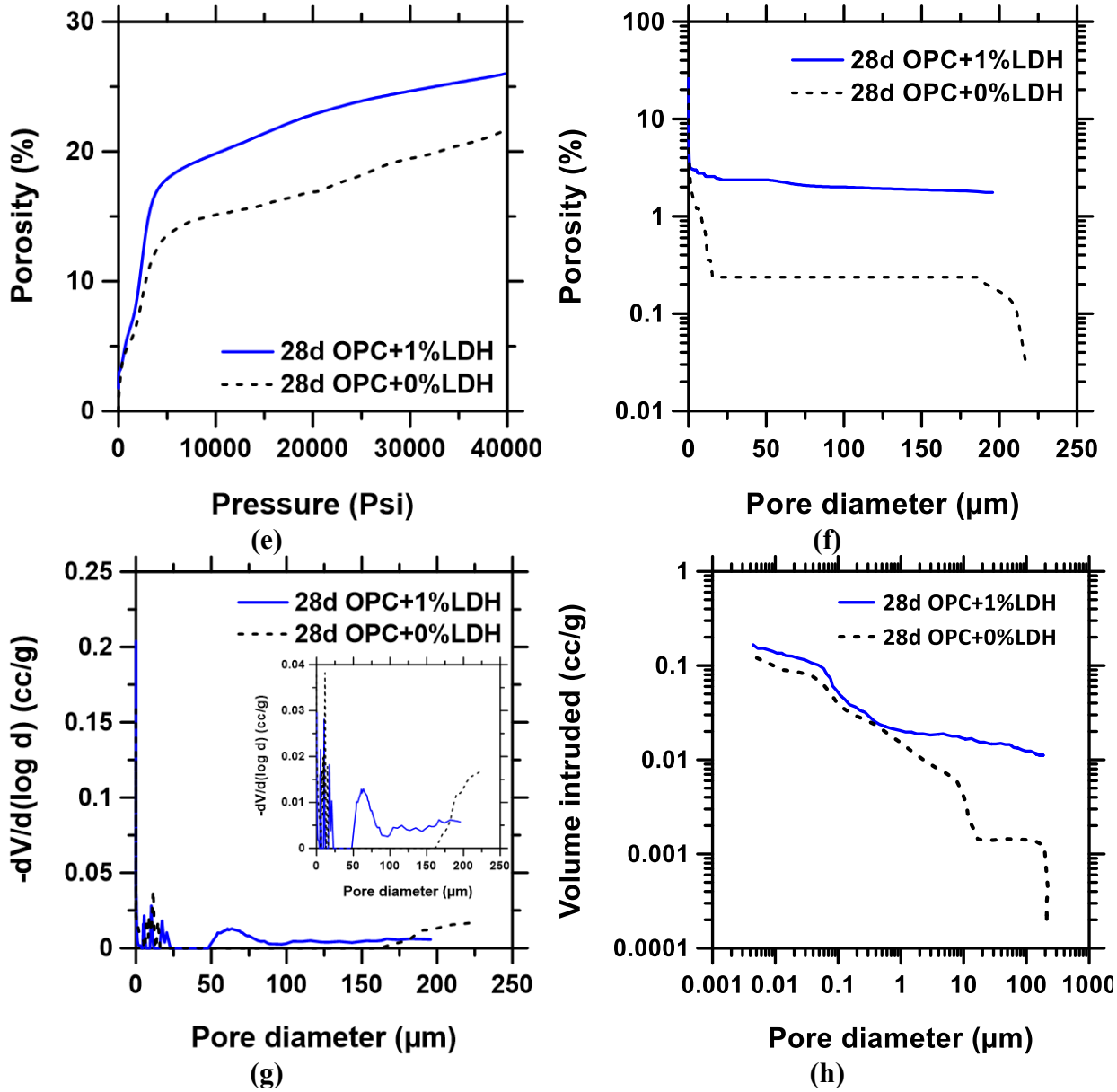

Fig. 14. Porosity and pore size distribution analysis of **(a, b, c, d)** 1d, and **(e, f, g, h)** 28d control and 1% LDH-dosed OPC cement samples. All the samples were prepared with the same designed mix proportions.

519

520

Table 4. Porosity of blended cement samples

Materials (with admixtures)	**Porosity (%)**
1d-OPC+0%LDH	35.94
1d-OPC+1%LDH	35.71
1d-CSA+0%LDH	24.94
1d-CSA+1%LDH	25.75

28d-OPC+0%LDH	21.62
28d-OPC+1%LDH	26.00
28d-CSA+0%LDH	20.54
28d-CSA+1%LDH	22.74

521

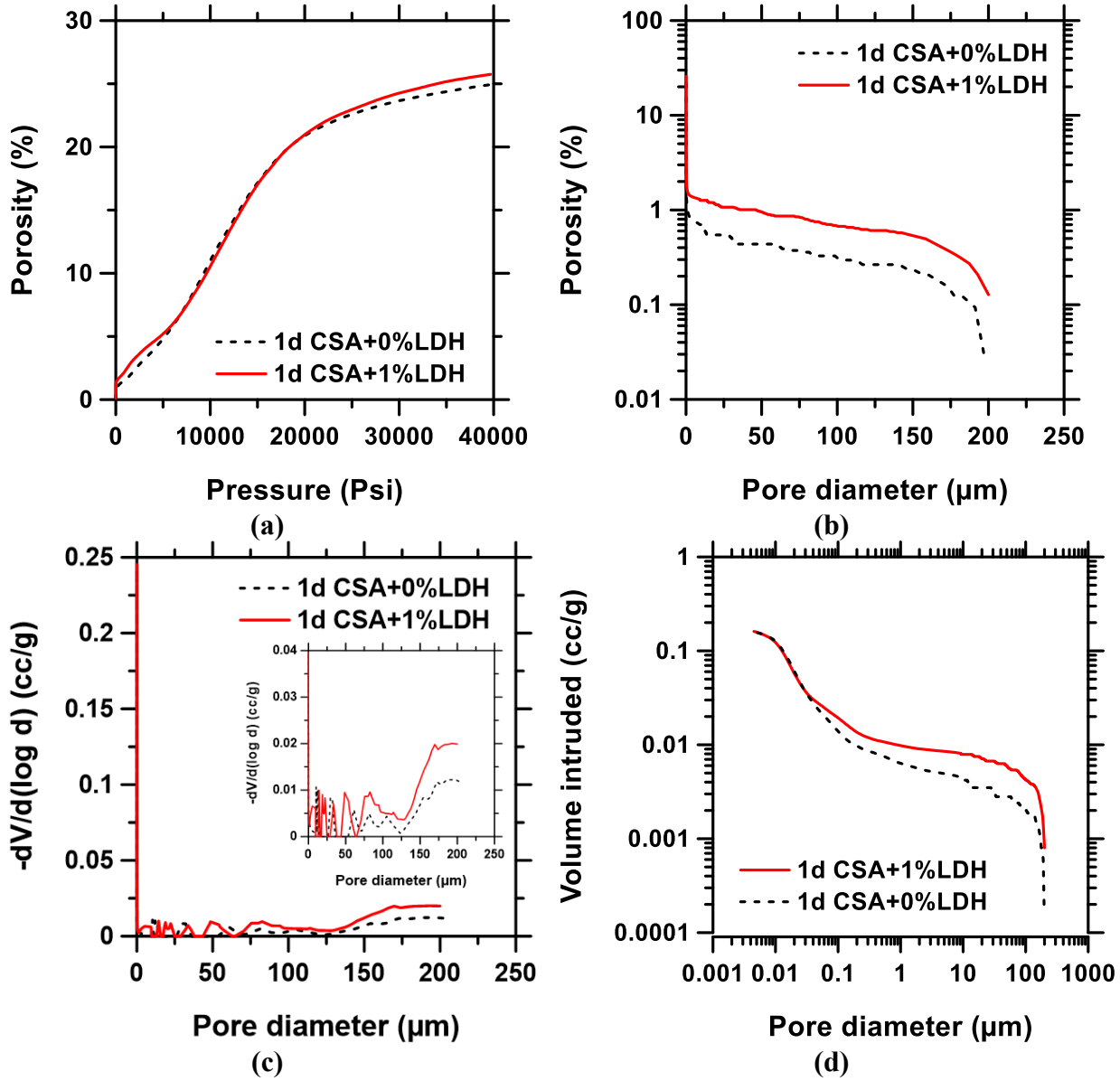

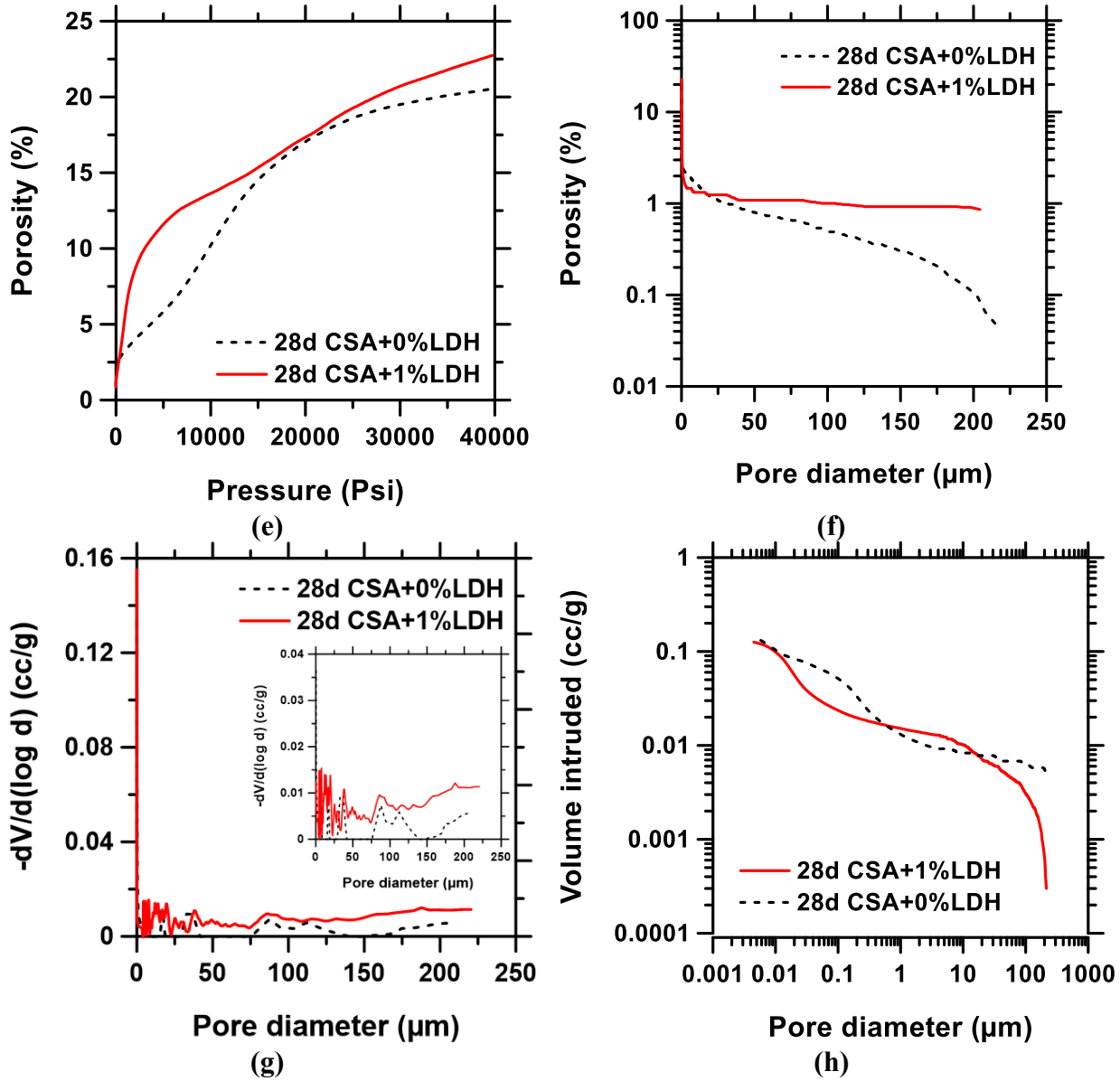

Fig. 15. Porosity and pore size distribution analysis of **(a, b, c, d)** 1d, and **(e, f, g, h)** 28d control and 1% LDH-dosed CSA cement samples. All the samples were prepared with the same designed mix proportions.

3.8. Compressive strength

The effect of CaAl-LDH on modified OPC and CSA cement paste can also be characterized by its impact on the compression resistance. **Fig. 16** represents the 1d and 28d compressive strength of OPC and CSA cement pastes with a 0% (control paste), 1% and 5% LDH dosage. The results indicate that CaAl-NO_3 LDH does not improve the mechanical strength in both 1d and 28d OPC and CSA cement cubes. A slight reduction continued with increase in the LDH content in the cement systems, which is slightly contrary to the results available in the literature [90]. However, addition of higher content of LDH (e.g., 1,5 - 10% LDH), and larger particle size of the LDH may affect the microstructure and results in lower compressive strength [46,90,91]. The reduction of strength in LDH-dosed OPC systems can be attributed to the calcite formation in the samples

shown in **Fig. 10 (a)**. The reduction of the compressive strength is also proportionally related to higher porosity and larger pores in the cement systems. The porosity and pore distributions are discussed in the previous section. The compressive strength of CSA cubes, shown in **Fig. 16 (b)** followed similar trends like OPC. However, the evolution of compressive strength in CSA samples seems lower than the published results [47,51], though Li and Mg-based LDHs were used in those studies. One possible reason can be the effect of admixtures, specifically the effect of retarder or combined negative effect of citric acid, PCE, and the LDH. Both the 1d and 28d porosimetry data discussed in **section 3.7** indicates that larger pores were present in the CSA samples, which could lead to the reduction in strength. Overall, higher dosage and larger particle sizes of LDH can cause agglomeration and may lead to decrease the strength, instead of enhancement of strength by LDH. As mechanical strength is one of the vital parameters for the assessment and acceptability of construction materials, further investigation is needed on the improvement of compressive strength. The possible areas of improvement can be the use of nano-LDH, lowering the CaAl-NO_3 LDH content (e.g., ≤ 1% dosage), enhancing dispersion, and increasing the w/c ratio to fulfill the water demand for the completion of hydration reaction.

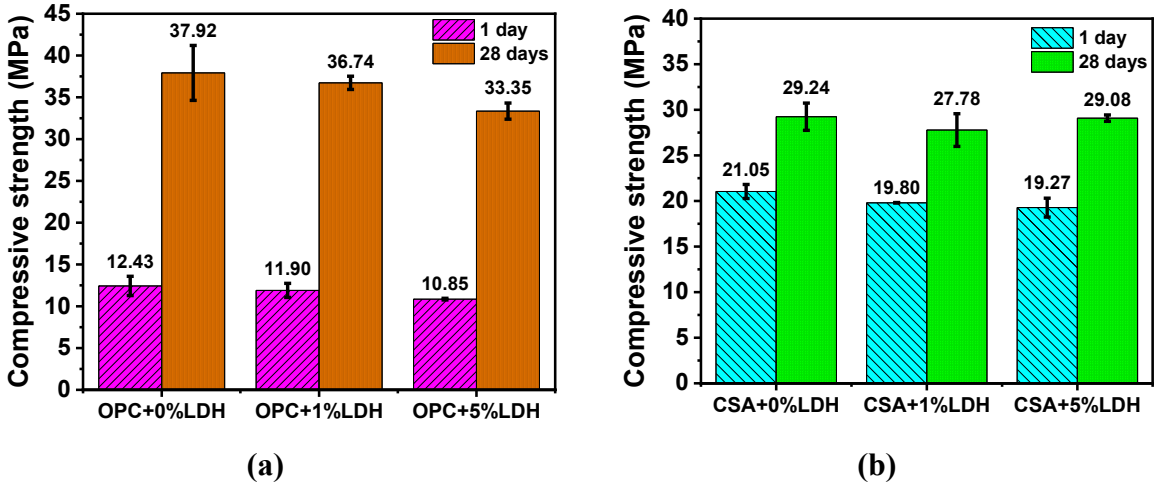

Fig. 16. Compressive strength of 0-5% LDH-dosed: (**a**) OPC, and (**b**) CSA cement pastes. Similar mix design proportions were used to make all the pastes' cubes.

4. Conclusions

The study examined the impact of submicron CaAl-NO_3 LDH particles on the properties of OPC and CSA cement pastes in both their fresh and mature stages, and following conclusions can be drawn.

(1) Rheology-based protocol was employed to investigate the time-dependent quantitative workability of cement pastes utilizing both static and dynamic yield stress modes. The outcomes indicate that LDH as a seeding agent providing crystal nuclei in the suspension and helps accelerate the hydration process by contributing more surface area for the nucleation and growth of the hydrated cement phases. Thus, in general, LDH in both cement

systems increased the flowability loss rate ($\boldsymbol{m_1}$), hardening rate ($\boldsymbol{m_2}$), yield stress growth rate constant ($\boldsymbol{k}$), acceleration angle ($\boldsymbol{\theta_p}$), and reduced the placement limit ($\boldsymbol{t_p}$).

(2) Over a 28-day tracking of the evolution of hydrated phase assemblage, it was revealed that the LDH-dosed OPC showed quicker depletion of gypsum and more rapid formation of ettringite, along with a slight increase in calcite precipitation compared to the control. This indicates that LDH seeding accelerated the hydration process. In the context of CSA pastes, LDH peaks were clearly present as early as 0.5 h in the LDH-dosed system, however, there was no significant impact of the LDH on the CSA's overall mineral phase assemblage.

(3) Isothermal calorimetry findings affirm a more pronounced seeding effect of LDH on OPC than CSA cement pastes, accelerating the hydration reactions. As anticipated, higher LDH dosing (1 to 5 $\%_{mass}$) in CSA systems corresponded with increased heat production. In contrast, addition of LDH to OPC systems resulted in reduced peak heat flow and cumulative heat generation. The observed endothermic properties of OPC pastes might be slightly enhanced due to calcite formation, and the dominance of a reaction pathway with lower enthalpy of formation. This discovery can be advantageous for additive concrete manufacturing, such as 3D printing, where a balance between rapid setting post-placement, improved thixotropy, and reduced heat generation is desirable.

(4) LDH addition slightly reduced compressive strengths attributable to increase in porosity, presence of larger pores, highlighting the negative impact of CaAl-NO_3 LDH. Nevertheless, these systems can benefit applications requiring rapid hardening, even if it slightly reduces concrete's strength.

Further research is crucial to fully understand the role of CaAl-NO_3 LDH in construction materials. Recommendations for future work include studying the effect of nano-sized LDH particles, limiting LDH dosage below 1%, altering admixtures, enhancing dispersion, tracking the performances for an extended period (e.g., several months), applying these materials in challenging environments, and employing molecular simulation to uncover detailed interactions and phase formations.

Acknowledgments

The authors acknowledge financial support from National Science Foundation through CMMI: 1932690. The contents of this paper reflect the views and opinions of the authors, who are responsible for the accuracy of data presented herein. The authors are thankful to Sanaa Tber of GCP Applied Technologies, USA; Stewart Parker of Continental Cement Co.; and William Bill Krupa of Buzzi Unicem USA for providing test materials. The author appreciates the instrumental support from the Materials Research Center (MRC) at Missouri S&T. All supports that enable the operation of the Okoronkwo's SusMatLab are acknowledged. The authors also would like to acknowledge Carrie Clinton for her contribution in the rheology experiments, and Dr. Wenyu Liao for his critical cooperation on the MIP instrument. The contents of this paper reflect the views and opinions of the authors, who are responsible for the accuracy of data presented herein.

References

[1] D.G. Evans, R.C. Slade, Structural aspects of layered double hydroxides, Layered Double Hydroxides (2006) 1–87.

[2] F. Cavani, F. Trifiro, A. Vaccari, Hydrotalcite-type anionic clays: Preparation, properties and applications., Catalysis Today 11 (1991) 173–301.

[3] X. Wang, J. Zhu, F. Zou, N. Zhou, Y. Zhong, CaAl–NO2 LDH hybrid self-healing microcapsules with chloride triggering: Towards synergistic corrosion resistance, Composites Part B: Engineering 264 (2023) 110902.

[4] M. Takemoto, Y. Tokudome, H. Murata, K. Okada, M. Takahashi, A. Nakahira, Synthesis of high-specific-surface-area Li-Al mixed metal oxide: Through nanoseed-assisted growth of layered double hydroxide, Applied Clay Science 203 (2021) 106006.

[5] M.U. Okoronkwo, M. Balonis, M. Juenger, M. Bauchy, N. Neithalath, G. Sant, Stability of Calcium–Alumino Layered-Double-Hydroxide Nanocomposites in Aqueous Electrolytes, Ind. Eng. Chem. Res. 57 (2018) 13417–13426. https://doi.org/10.1021/acs.iecr.8b02618.

[6] L. Yang, P. Zhao, C. Liang, M. Chen, L. Niu, J. Xu, D. Sun, L. Lu, Characterization and adaptability of layered double hydroxides in cement paste, Applied Clay Science 211 (2021) 106197.

[7] A.A. Bhattacharyya, G.M. Woltermann, J.S. Yoo, J.A. Karch, W.E. Cormier, Catalytic SOx abatement: the role of magnesium aluminate spinel in the removal of SOx from fluid catalytic cracking (FCC) flue gas, Industrial & Engineering Chemistry Research 27 (1988) 1356–1360.

[8] J.S. Yoo, A.A. Bhattacharyya, C.A. Radlowski, De-SOx catalyst: an XRD study of magnesium aluminate spinel and its solid solutions, Industrial & Engineering Chemistry Research 30 (1991) 1444–1448.

[9] D.L. Bish, Anion-exchange in takovite: applications to other hydroxide minerals, Bulletin de Mineralogie 103 (1980) 170–175.

[10] D. Yang, S. Song, Y. Zou, X. Wang, S. Yu, T. Wen, H. Wang, T. Hayat, A. Alsaedi, X. Wang, Rational design and synthesis of monodispersed hierarchical SiO2@ layered double hydroxide nanocomposites for efficient removal of pollutants from aqueous solution, Chemical Engineering Journal 323 (2017) 143–152.

[11] M.B. Poudel, G.P. Awasthi, H.J. Kim, Novel insight into the adsorption of Cr (VI) and Pb (II) ions by MOF derived Co-Al layered double hydroxide@ hematite nanorods on 3D porous carbon nanofiber network, Chemical Engineering Journal 417 (2021) 129312.

[12] L. Feng, Q. Zhang, F. Ji, L. Jiang, C. Liu, Q. Shen, Q. Liu, Phosphate removal performances of layered double hydroxides (LDH) embedded polyvinyl alcohol/lanthanum alginate hydrogels, Chemical Engineering Journal 430 (2022) 132754.

[13] Jettka W, Gajdos B, Benedikt MD, Eur. Patent EP, 715846, 1996.

[14] Miyata S, US Patent, 1985.

[15] J.-H. Choy, S.-Y. Kwak, J.-S. Park, Y.-J. Jeong, J. Portier, Intercalative nanohybrids of nucleoside monophosphates and DNA in layered metal hydroxide, Journal of the American Chemical Society 121 (1999) 1399–1400.

[16] S.-Y. Kwak, Y.-J. Jeong, J.-S. Park, J.-H. Choy, Bio-LDH nanohybrid for gene therapy, Solid State Ionics 151 (2002) 229–234.

[17] A. Merz, Chemically modified electrodes, in: Electrochemistry IV, Springer, 1990: pp. 49–90.

[18] X. Wang, J. Zhu, F. Zou, N. Zhou, Y. Li, W. Lei, Ca-Al LDH hybrid self-healing microcapsules for corrosion protection, Chemical Engineering Journal (2022) 137125.

[19] L. Ma, Y. Qiang, W. Zhao, Designing novel organic inhibitor loaded MgAl-LDHs nanocontainer for enhanced corrosion resistance, Chemical Engineering Journal 408 (2021) 127367.

[20] J. Wei, J. Xu, Y. Mei, Q. Tan, Chloride adsorption on aminobenzoate intercalated layered double hydroxides: Kinetic, thermodynamic and equilibrium studies, Applied Clay Science 187 (2020) 105495.
[21] X. Ke, S.A. Bernal, J.L. Provis, Uptake of chloride and carbonate by Mg-Al and Ca-Al layered double hydroxides in simulated pore solutions of alkali-activated slag cement, Cement and Concrete Research 100 (2017) 1–13.
[22] J. Xu, Y. Song, Y. Zhao, L. Jiang, Y. Mei, P. Chen, Chloride removal and corrosion inhibitions of nitrate, nitrite-intercalated MgAl layered double hydroxides on steel in saturated calcium hydroxide solution, Applied Clay Science 163 (2018) 129–136.
[23] E. Constable, Comprehensive Supramolecular Chemistry, Polynuclear Transition Metal Helicates 9 (1996) 213.
[24] A. Vaccari, Preparation and catalytic properties of cationic and anionic clays, Catalysis Today 41 (1998) 53–71.
[25] L. Van der Ven, M. Van Gemert, L. Batenburg, J. Keern, L. Gielgens, T. Koster, H. Fischer, On the action of hydrotalcite-like clay materials as stabilizers in polyvinylchloride, Applied Clay Science 17 (2000) 25–34.
[26] L. Raki, J. Beaudoin, R. Alizadeh, J. Makar, T. Sato, Cement and concrete nanoscience and nanotechnology, Materials 3 (2010) 918–942.
[27] Z.M. Mir, A. Bastos, D. Höche, M.L. Zheludkevich, Recent Advances on the Application of Layered Double Hydroxides in Concrete—A Review, Materials 13 (2020) 1426.
[28] L. Raki, J. Beaudoin, L. Mitchell, Layered double hydroxide-like materials: nanocomposites for use in concrete, Cement and Concrete Research 34 (2004) 1717–1724.
[29] Z. Yang, H. Fischer, R. Polder, Possibilities for improving corrosion protection of reinforced concrete by modified hydrotalcites–a literature review, Advances in Modeling Concrete Service Life (2012) 95–105.
[30] Z. Yang, H. Fischer, R. Polder, Modified hydrotalcites as a new emerging class of smart additive of reinforced concrete for anticorrosion applications: A literature review, Materials and Corrosion 64 (2013) 1066–1074.
[31] Y. Xu, B. Lin, X. Yu, S.-T. Li, Influence of MgAl-LDHs/TiO2 composites on the mechanical and photocatalytic properties of cement pastes and recycled aggregates, Construction and Building Materials 377 (2023) 131122.
[32] Z. Yang, Y. Xu, X. Cai, J. Wu, J. Wang, Studying properties of pervious concrete containing recycled aggregate loaded with TiO2/LDHs and its liquid pollutant purification, Construction and Building Materials 406 (2023) 133398. https://doi.org/10.1016/j.conbuildmat.2023.133398.
[33] A.A.H. Faisal, A.H. Shihab, Mu. Naushad, T. Ahamad, G. Sharma, K.M. Al-Sheetan, Green synthesis for novel sorbent of sand coated with (Ca/Al)-layered double hydroxide for the removal of toxic dye from aqueous environment, Journal of Environmental Chemical Engineering 9 (2021) 105342. https://doi.org/10.1016/j.jece.2021.105342.
[34] A. Singha Roy, S. Kesavan Pillai, S.S. Ray, Layered double hydroxides for sustainable agriculture and environment: An overview, ACS Omega 7 (2022) 20428–20440.
[35] R. Sharma, G.G.C. Arizaga, A.K. Saini, P. Shandilya, Layered double hydroxide as multifunctional materials for environmental remediation: from chemical pollutants to microorganisms, Sustainable Materials and Technologies 29 (2021) e00319.
[36] D. Fu, T.A. Kurniawan, R. Avtar, P. Xu, M.H.D. Othman, Recovering heavy metals from electroplating wastewater and their conversion into Zn2Cr-layered double hydroxide (LDH) for pyrophosphate removal from industrial wastewater, Chemosphere 271 (2021) 129861. https://doi.org/10.1016/j.chemosphere.2021.129861.

[37] A. Mohajerani, L. Burnett, J.V. Smith, H. Kurmus, J. Milas, A. Arulrajah, S. Horpibulsuk, A. Abdul Kadir, Nanoparticles in Construction Materials and Other Applications, and Implications of Nanoparticle Use, Materials 12 (2019) 3052. https://doi.org/10.3390/ma12193052.
[38] T. Matschei, B. Lothenbach, F.P. Glasser, The AFm phase in Portland cement, Cement and Concrete Research 37 (2007) 118–130. https://doi.org/10.1016/j.cemconres.2006.10.010.
[39] M.U. Okoronkwo, Phase development in cement hydrate systems, Ph.D. Thesis, University of Aberdeen, UK, 2014. https://abdn.alma.exlibrisgroup.com/discovery/delivery/44ABE_INST:44ABE_VU1/12152387470005941 (accessed July 13, 2021).
[40] M.U. Okoronkwo, F.P. Glasser, Compatibility of hydrogarnet, Ca3Al2(SiO4)x(OH)4(3−x), with sulfate and carbonate-bearing cement phases: 5–85°C, Cement and Concrete Research 83 (2016) 86–96. https://doi.org/10.1016/j.cemconres.2016.01.013.
[41] M.U. Okoronkwo, F.P. Glasser, Stability of strätlingite in the CASH system, Mater Struct 49 (2016) 4305–4318. https://doi.org/10.1617/s11527-015-0789-x.
[42] M.U. Okoronkwo, F.P. Glasser, Strätlingite: compatibility with sulfate and carbonate cement phases, Mater Struct 49 (2016) 3569–3577. https://doi.org/10.1617/s11527-015-0740-1.
[43] M. Balonis, M. Mędala, F.P. Glasser, Influence of calcium nitrate and nitrite on the constitution of AFm and AFt cement hydrates, Advances in Cement Research 23 (2011) 129–143. https://doi.org/10.1680/adcr.10.00002.
[44] M. Juenger, F. Winnefeld, J.L. Provis, J. Ideker, Advances in alternative cementitious binders, Cement and Concrete Research 41 (2011) 1232–1243.
[45] Y. Tao, A. Rahul, M.K. Mohan, G. De Schutter, K. Van Tittelboom, Recent progress and technical challenges in using calcium sulfoaluminate (CSA) cement, Cement and Concrete Composites (2022) 104908.
[46] C.-W. Chung, H.-Y. Jung, J.-H. Kwon, B.-K. Jang, J.-H. Kim, Use of calcium aluminum–layered double hydroxide to control chloride ion penetration of cement-based materials, Journal of Structural Integrity and Maintenance 4 (2019) 37–42.
[47] P. Duan, W. Chen, J. Ma, Z. Shui, Influence of layered double hydroxides on microstructure and carbonation resistance of sulphoaluminate cement concrete, Construction and Building Materials 48 (2013) 601–609.
[48] M.A. Yazdi, E. Gruyaert, K. Van Tittelboom, N. De Belie, New findings on the contribution of Mg-Al-NO3 layered double hydroxides to the hydration and chloride binding capacity of cement pastes, Cement and Concrete Research 163 (2023) 107037.
[49] S. Xu, Z. Chen, B. Zhang, J. Yu, F. Zhang, D.G. Evans, Facile preparation of pure CaAl-layered double hydroxides and their application as a hardening accelerator in concrete, Chemical Engineering Journal 155 (2009) 881–885.
[50] L. Cao, J. Guo, J. Tian, Y. Xu, M. Hu, M. Wang, J. Fan, Preparation of Ca/Al-layered double hydroxide and the influence of their structure on early strength of cement, Construction and Building Materials 184 (2018) 203–214.
[51] D. Zou, K. Wang, H. Li, X. Guan, Effect of LiAl-layered double hydroxides on hydration of calcium sulfoaluminate cement at low temperature, Construction and Building Materials 223 (2019) 910–917.
[52] A. Wongariyakawee, Novel layered double hydroxide chemistry for application in cement and other building materials, Ph.D. Thesis, University of Oxford, UK, (2013).
[53] J.D. Mangadlao, P. Cao, R.C. Advincula, Smart cements and cement additives for oil and gas operations, Journal of Petroleum Science and Engineering 129 (2015) 63–76.
[54] M. Meyn, K. Beneke, G. Lagaly, Anion-exchange reactions of layered double hydroxides, Inorganic Chemistry 29 (1990) 5201–5207.

[55] F. Millange, R.I. Walton, L. Lei, D. O 'Hare, Efficient separation of terephthalate and phthalate anions by selective ion-exchange intercalation in the layered double hydroxide Ca2Al (OH) 6⊙ NO3⊙ 2H2O, Chemistry of Materials 12 (2000) 1990–1994.
[56] H.M. Rietveld, A profile refinement method for nuclear and magnetic structures, Journal of Applied Crystallography 2 (1969) 65–71. https://doi.org/10.1107/S0021889869006558.
[57] H.M. Rietveld, Line profiles of neutron powder-diffraction peaks for structure refinement, Acta Cryst 22 (1967) 151–152. https://doi.org/10.1107/S0365110X67000234.
[58] R. Belhadi, A. Govin, P. Grosseau, Influence of polycarboxylate superplasticizer, citric acid and their combination on the hydration and workability of calcium sulfoaluminate cement, Cement and Concrete Research 147 (2021) 106513. https://doi.org/10.1016/j.cemconres.2021.106513.
[59] P. Zhou, J. Xu, M.-Z. Guo, Z. Wang, Laboratory investigation of the chloride ingress into cement mortar incorporating a novel core–shell nanomaterial, Construction and Building Materials 379 (2023) 131306.
[60] S.K. Mondal, A. Welz, C. Clinton, K. Khayat, A. Kumar, M.U. Okoronkwo, Quantifying the Workability of Calcium Sulfoaluminate Cement Paste Using Time-Dependent Rheology, Materials 15 (2022) 5775.
[61] TA Instruments, Ten steps to a better rheological measurement — TA rheology training seminar, (n.d.). http://www.chem.mtu.edu/~fmorriso/cm4655/TAInstruments/2013TA_ 10stepstogoodrheolmeasurements.pdf2005.
[62] M. Yang, H. Jennings, Influences of mixing methods on the microstructure and rheological behavior of cement paste, Advanced Cement Based Materials 2 (1995) 70–78.
[63] P.F.G. Banfill, Rheology of Fresh Cement and Concrete: Proceedings of an International Conference, Liverpool, 1990, CRC Press, 1990.
[64] M. Nehdi, M.-A. Rahman, Estimating rheological properties of cement pastes using various rheological models for different test geometry, gap and surface friction, Cement and Concrete Research 34 (2004) 1993–2007.
[65] F.A. Cardoso, A.L. Fujii, R.G. Pileggi, M. Chaouche, Parallel-plate rotational rheometry of cement paste: Influence of the squeeze velocity during gap positioning, Cement and Concrete Research 75 (2015) 66–74. https://doi.org/10.1016/j.cemconres.2015.04.010.
[66] P. Coussot, Rheometry of pastes, suspensions, and granular materials: applications in industry and environment, John Wiley & Sons, 2005.
[67] Q. Nguyen, D. Boger, Measuring the flow properties of yield stress fluids, Annual Review of Fluid Mechanics 24 (1992) 47–88.
[68] G. Sant, C.F. Ferraris, J. Weiss, Rheological properties of cement pastes: a discussion of structure formation and mechanical property development, Cement and Concrete Research 38 (2008) 1286–1296.
[69] M.U. Okoronkwo, G. Falzone, A. Wada, W. Franke, N. Neithalath, G. Sant, Rheology-based protocol to establish admixture compatibility in dense cementitious suspensions, Journal of Materials in Civil Engineering 30 (2018) 04018122.
[70] O. Linderoth, L. Wadsö, D. Jansen, Long-term cement hydration studies with isothermal calorimetry, Cement and Concrete Research 141 (2021) 106344.
[71] J.M.V. Gómez-Soberón, Porosity of recycled concrete with substitution of recycled concrete aggregate: An experimental study, Cement and Concrete Research 32 (2002) 1301–1311. https://doi.org/10.1016/S0008-8846(02)00795-0.
[72] I. Galan, H. Beltagui, M. García-Maté, F.P. Glasser, M.S. Imbabi, Impact of drying on pore structures in ettringite-rich cements, Cement and Concrete Research 84 (2016) 85–94. https://doi.org/10.1016/j.cemconres.2016.03.003.
[73] E.W. Washburn, The dynamics of capillary flow, Physical Review 17 (1921) 273.

[74] H. Ma, Mercury intrusion porosimetry in concrete technology: tips in measurement, pore structure parameter acquisition and application, Journal of Porous Materials 21 (2014) 207–215.
[75] F. Moro, H. Böhni, Ink-bottle effect in mercury intrusion porosimetry of cement-based materials, Journal of Colloid and Interface Science 246 (2002) 135–149.
[76] S. Diamond, Mercury porosimetry: An inappropriate method for the measurement of pore size distributions in cement-based materials, Cement and Concrete Research 30 (2000) 1517–1525.
[77] Y. Wu, P. Duan, C. Yan, Role of layered double hydroxides in setting, hydration degree, microstructure and compressive strength of cement paste, Applied Clay Science 158 (2018) 123–131.
[78] D. Marchon, S. Mantellato, A.B. Eberhardt, R.J. Flatt, Adsorption of chemical admixtures, in: Science and Technology of Concrete Admixtures, Elsevier, 2016: pp. 219–256.
[79] T. Su, X. Kong, H. Tian, D. Wang, Effects of comb-like PCE and linear copolymers on workability and early hydration of a calcium sulfoaluminate belite cement, Cement and Concrete Research 123 (2019) 105801.
[80] G. Li, T. He, D. Hu, C. Shi, Effects of two retarders on the fluidity of pastes plasticized with aminosulfonic acid-based superplasticizers, Construction and Building Materials 26 (2012) 72–78.
[81] G. Gelardi, R. Flatt, Working mechanisms of water reducers and superplasticizers, in: Science and Technology of Concrete Admixtures, Elsevier, 2016: pp. 257–278.
[82] L. Raki, J.J. Beaudoin, Controlled release of chemical admixtures, (2011).
[83] N. Roussel, A thixotropy model for fresh fluid concretes: theory, validation and applications, Cement and Concrete Research 36 (2006) 1797–1806.
[84] A. Papo, L. Piani, Effect of various superplasticizers on the rheological properties of Portland cement pastes, Cement and Concrete Research 34 (2004) 2097–2101.
[85] N. Roussel, A theoretical frame to study stability of fresh concrete, Materials and Structures 39 (2006) 81–91.
[86] J.H. Kim, M. Beacraft, S.P. Shah, Effect of mineral admixtures on formwork pressure of self-consolidating concrete, Cement and Concrete Composites 32 (2010) 665–671.
[87] P.R. de Matos, R. Pilar, C.A. Casagrande, P.J.P. Gleize, F. Pelisser, Comparison between methods for determining the yield stress of cement pastes, Journal of the Brazilian Society of Mechanical Sciences and Engineering 42 (2020) 1–13.
[88] H. Li, X. Guan, L. Yang, S. Liu, J. Zhang, Y. Guo, Effects of LiAl-layered double hydroxides on early hydration of calcium sulphoaluminate cement paste, Journal of Wuhan University of Technology-Mater. Sci. Ed. 32 (2017) 1101–1107.
[89] H. Li, K. Yang, X. Guan, Effect of water-to-binder ratio on the properties of CSA cement-based grouting materials with LiAl-LDH, Advanced Composites Letters 29 (2020) 2633366X20908876.
[90] Z. Qu, Q. Yu, H. Brouwers, Relationship between the particle size and dosage of LDHs and concrete resistance against chloride ingress, Cement and Concrete Research 105 (2018) 81–90.
[91] S. Zhang, F. Yu, W. He, D. Zheng, H. Cui, L. Lv, W. Tang, N. Han, Experimental investigation of chloride uptake performances of hydrocalumite-like Ca-Al LDHs with different microstructures, Applied Sciences 10 (2020) 3760.
[92] A. Noumowé, Effet des hautes températures (20 °C–600 °C) sur le béton, PhD thesis, Institut National des Sciences Appliquées, 1995.
[93] G. Platret, Suivi de l'hydratation du ciment et de l'évolution des phases solides dans les bétons par analyse thermique, caractéristiques microstructurales et propriétés relativesa la durabilité des bétons. méthodes de mesure et d'essai de laboratoire, Méthode d'essai 58 (2002).
[94] Q. Zhou, F.P. Glasser, Thermal stability and decomposition mechanisms of ettringite at< 120 C, Cement and Concrete Research 31 (2001) 1333–1339.

[95] E. Nonnet, N. Lequeux, P. Boch, Elastic properties of high alumina cement castables from room temperature to 1600 C, Journal of the European Ceramic Society 19 (1999) 1575–1583.
[96] N. Richard, Structure et proprietes elastiques des phases cimentieres base de mono-aluminate de calcium, (1996).
[97] G. Khoury, Compressive strength of concrete at high temperatures: a reassessment, Magazine of Concrete Research 44 (1992) 291–309.
[98] P. Grattan-Bellew, Microstructural investigation of deteriorated Portland cement concretes, Construction and Building Materials 10 (1996) 3–16.
[99] M. Fridrichová, K. Dvořák, D. Gazdič, J. Mokrá, K. Kulísek, Thermodynamic Stability of Ettringite Formed by Hydration of Ye'elimite Clinker, Advances in Materials Science and Engineering 2016 (2016) e9280131. https://doi.org/10.1155/2016/9280131.
[100] K. Ogawa, D.M. Roy, C4A3S hydration ettringite formation, and its expansion mechanism: I. expansion; Ettringite stability, Cement and Concrete Research 11 (1981) 741–750. https://doi.org/10.1016/0008-8846(81)90032-6.
[101] A. Leemann, R. Loser, B. Münch, Influence of cement type on ITZ porosity and chloride resistance of self-compacting concrete, Cement and Concrete Composites 32 (2010) 116–120. https://doi.org/10.1016/j.cemconcomp.2009.11.007.
[102] W. Liao, A. Kumar, K. Khayat, H. Ma, Multifunctional lightweight aggregate containing phase change material and water for damage mitigation of concrete, ES Materials & Manufacturing 6 (2019) 49–61. http://dx.doi.org/10.30919/esmm5f606.
[103] J. Liu, F. Xing, B. Dong, H. Ma, D. Pan, Study on water sorptivity of the surface layer of concrete, Materials and Structures 47 (2014) 1941–1951.
[104] S. Bahafid, A multi-technique investigation of the effect of hydration temperature on the microstructure and mechanical properties of cement paste, Doctoral Dissertation, University Paris Est (2017). https://www.theses.fr/2017PESC1021.